

Static Dark Fluid Thin Shells in Schwarzschild-de Sitter Spacetimes: Stability and Black Hole Shadows

Dimitrios Efstratiou,^{1,*} Evangelos Achilleas Paraskevas,^{1,†} and Leandros Perivolaropoulos^{1,‡}

¹*Department of Physics, University of Ioannina, GR-45110, Ioannina, Greece*

(Dated: February 26, 2026)

We investigate the existence and radial stability of static, spherically symmetric thin shells separating two Schwarzschild–de Sitter spacetimes with distinct parameters (m_{\pm}, Λ_{\pm}) . Using the Israel junction formalism and a linear barotropic equation of state $p = \lambda(\sigma - \sigma_1)c^2$, we decouple the sound speed $c_s^2 = \lambda c^2$ from the stable equilibrium equation-of-state parameter $w_0 \equiv p_0/(\sigma_0 c^2)$ and derive the effective potential governing radial dynamics. For observationally motivated parameters, stable configurations with $\sigma_0 > 0$ and $0 < \lambda \leq 1$ exist only when $m_+/m_- > 1$. Three distinct stability windows emerge, when $\lambda = 1$: $-3/7 \lesssim w_0 \lesssim 1/2$ for $\Lambda_+ = \Lambda_-$; $-2/3 \lesssim w_0 \lesssim 1/2$ for $\Lambda_+ > \Lambda_-$; and $0 \lesssim w_0 \lesssim 1$ for $\Lambda_+ < \Lambda_-$. Positive-pressure shells ($w_0 > 0$) reside near the photon sphere, whereas negative-pressure shells ($w_0 < 0$) extend outward, reaching either the cosmological horizon or the static radius. Stability relies on the variation of $w(\sigma)$ with the surface energy density. Negative pressure (tension) stabilizes the system because the tension increases during expansion. Conversely, positive pressure stabilizes the system because the pressure increases during contraction. Finally, a static, stable, dark, fluid thin shell acts as a gravitational refractive layer that enlarges the black hole’s shadow for a distant, static observer outside the shell. The effect depends on the shell radius R_0 , the background parameters (m_{\pm}, Λ_{\pm}) , and the equation-of-state. Dark fluid shells can be considered as theoretical toy models that illustrate qualitative effects. Future high-resolution black hole shadow observations could, in principle, use such models to explore how different equations of state might influence observable signatures.

I. INTRODUCTION

Thin shells in spherically symmetric static spacetimes serve as a valuable idealization in general relativity. They are frequently used to model processes such as gravitational collapse [1], as well as to investigate physical mechanisms involving domain walls [2–6] and braneworld scenarios [7–9]. Israel’s junction formalism [10] gives a systematic method for constructing such shells by matching two spacetime manifolds across a timelike hypersurface identified with the shell. In this framework, the induced metric is continuous across the junction, while the extrinsic curvature is discontinuous, with the jump encoding the stress–energy content localized on the shell. For comprehensive treatments of the thin-shell junction formalism, see, for instance, [11–13]. An exact static thin-shell solution surrounding a black hole was obtained by Frauendiener *et al.* [14], and its stability was later analysed in Refs. [15, 16].

Models of thin shells have been used to examine stellar structures or gravastars [17–22] or cosmological bubbles [23–25]. Analyses of spherically symmetric thin shells have focused on their stability [1, 4, 21, 26–31] and their gravitational collapse [32–35]. These constructions have been extended to alternative theories of gravity, including Gauss–Bonnet and $F(Q)$ gravity [36, 37]. In the context of scalar fields, gravitational collapse can lead to the formation of a thin shell [38], and the dynamics and

stability of such scalar field shells have also been investigated [39, 40]. Furthermore, rotating thin-shell configurations have been introduced [5, 41, 42], along with studies on the stability of charged thin shells [43, 44]. In addition, charge screening by thin shells in a $(2+1)$ -dimensional regular black hole spacetime was explored in Ref. [45]. Screening of the Reissner–Nordström charge by a dust thin shell was presented in Ref. [46]. The thermodynamic properties, entropy, and stability of thin shells in $(2+1)$ -dimensional flat spacetimes were investigated in Refs. [47, 48], while thin shells connecting local cloud-of-strings geometries were studied in Refs. [29, 49]. Furthermore, by applying the cut-and-paste procedure to two black hole spacetimes and removing the singular regions, one can create thin-shell wormholes supported by exotic matter at the throat [26, 50–72]. Recently, several works [73–81] have explored the observational signatures of thin shells and shell-like structures surrounding black holes, gravastars, and wormholes, as well as within modified gravity frameworks, focusing on their impact on strong-field gravitational lensing [82] and on the detailed morphology of black hole shadows and associated photon rings.

In this work, we analyze the existence and stability of static, spherically symmetric thin shells whose interior and exterior regions are described by Schwarzschild–de Sitter geometries, with possibly different mass parameters m_{\pm} and cosmological constants Λ_{\pm} . Previous comprehensive studies on static and stable thin shells or wormhole solutions in SdS or Anti–de Sitter backgrounds can be found in [4, 26, 35, 51, 68, 71, 83]. Employing the Israel junction formalism, we obtain the effective potential governing the radial dynamics of the shell by assum-

* d.efstratiou@uoi.gr

† e.paraskevas@uoi.gr

‡ leandros@uoi.gr

ing a linear barotropic equation of state, $p = \lambda(\sigma - \sigma_1)c^2$ (where σ_1 is a constant), which introduces an additional degree of freedom and permits a positive sound speed even in the presence of negative pressure [15, 84, 85]. We map the stability regions by identifying the equilibrium radii R_0 at which the shell is static and stable, together with the corresponding surface energy densities σ_0 , for various choices of (m_{\pm}, Λ_{\pm}) , the equilibrium pressure-to-density ratio $w_0 \equiv p_0/(\sigma_0 c^2)$, and the parameter λ , defined via the sound speed $c_s^2 = \partial p/\partial \sigma = \lambda c^2$, which is not required to satisfy $\lambda = w_0$.

We present a numerical study of static, linearly stable thin shells characterized by the parameters (λ, w_0) , where λ fixes the sound speed and w_0 the pressure at R_0 . These shells are constructed by matching Schwarzschild–de Sitter spacetimes with parameters (m_{\pm}, Λ_{\pm}) . Adopting cosmological constants compatible with the *Planck* 2018 results [86, 87], we determine the allowed ranges of the equilibrium radius R_0 and surface energy density σ_0 for which static configurations can exist, and show that stable shells may form at several characteristic scales: near the black-hole photon sphere, around the Schwarzschild–de Sitter *static radius* $R_{\text{st}} = (3Gm/c^2\Lambda)^{1/2}$, and in the vicinity of the cosmological horizon.

Several astrophysical mechanisms can perturb a static thin shell away from equilibrium [21, 22, 50, 88–91]. By perturbing the shell’s effective potential (see also bounded-excursion stability criterion[21]), we consider small-energy perturbations (assumed not to backreact on the background spacetime) to estimate the characteristic timescales of oscillations about the equilibrium radius.

We further explore observational consequences for black hole shadows [92]. By treating the shell as a gravitational boundary layer, we show that it modifies the standard Schwarzschild–de Sitter shadow [93, 94] for a static observer between the horizons. For example, dark matter distributions around massive black holes are reviewed in [95]. Early adiabatic growth models for slowly accreting black holes in non-rotating, spherically symmetric galaxies predict a final cusp with density $\rho(r) \sim r^{-3/2}$ [96, 97]. More generally, γ -models with $\rho(r) \sim r^{-\gamma}$ yield spikes of the form $\rho_{\text{final}}(r) \sim r^{-\gamma_{\text{sp}}}$, where $\gamma_{\text{sp}} = (9 - 2\gamma)/(4 - \gamma)$ [95, 98, 99]. This adiabatic framework has been applied to dark matter spikes around black holes [100], and later extended to relativistic settings [101]. In our phenomenological approach, Λ_+ and Λ_- are treated as free parameters, with the results mapping the space of possible configurations. The physically most conservative limit $\Lambda_+ = \Lambda_-$ is always included as a special case. The physical realization of a static thin shell separating spacetimes with distinct cosmological constants ($\Lambda_+ \neq \Lambda_-$) could potentially find its natural origin in the theory of phase transitions [102, 103]. In the standard Coleman-De Luccia formalism [104–112], the decay of a metastable false vacuum to a true vacuum proceeds via the nucleation of bubbles, where the interior and exterior regions correspond to different minima ϕ_{\pm} of a scalar potential $V(\phi)$. The shell itself may represent the

domain wall where the scalar field interpolates between these vacuum expectation values. In a well-motivated physical scenario, a static, stable dark fluid thin shell could serve as a simple toy model for a dark matter or a domain wall configuration. Its imprint on the black hole shadow, combined with future high-resolution observations (e.g., [113–120]), could be used to constrain the shell’s equation-of-state parameter and to test models of such dark fluid configurations.

The structure of this work proceeds as follows. In Section II, we introduce the mathematical framework for analyzing the radial stability of a static thin shell of linear equation of state within a Schwarzschild–de Sitter spacetime characterized by parameters (m_{\pm}, Λ_{\pm}) . This includes deriving the appropriate junction conditions and constructing the effective potential. A systematic stability analysis is subsequently conducted via the construction of stability maps. In Section III, we study small-energy perturbations of the shell’s effective potential—assumed not to backreact on the background spacetime—in order to estimate the characteristic oscillation timescales about the equilibrium radius. In Section IV, we investigate potential observational signatures arising from deviations in the shadow of a Schwarzschild–de Sitter black hole caused by the presence of the thin shell. Finally, in Section V, we summarize our main findings and discuss their implications for astrophysical and cosmological models.

II. RADIAL STABILITY OF STATIC THIN SHELLS IN SCHWARZSCHILD–DE SITTER GEOMETRY

Let \mathcal{M} denote the spacetime and let $\Sigma \subset \mathcal{M}$ be a time-like hypersurface. We consider Σ as a spherically symmetric thin shell which separates two Schwarzschild–de Sitter regions, $\mathcal{M} = \mathcal{M}^+ \cup \mathcal{M}^-$, with $\partial\mathcal{M}^+ \cap \partial\mathcal{M}^- = \Sigma$. The two sides may carry different mass parameters m_{\pm} and different cosmological constants Λ_{\pm} . The metric on each side is static, spherically symmetric and satisfies the vacuum Einstein equations ($R_{\mu\nu}^{\pm} = \Lambda_{\pm} g_{\mu\nu}^{\pm}$) with cosmological constant¹

$$ds_{\pm}^2 = c^2 f_{\pm}(r_{\pm}) dt_{\pm}^2 - \frac{dr_{\pm}^2}{f_{\pm}(r_{\pm})} - r_{\pm}^2 (d\theta^2 + \sin^2 \theta d\phi^2), \quad (1)$$

with

$$f_{\pm}(r_{\pm}) = 1 - \frac{2Gm_{\pm}}{c^2 r_{\pm}} - \frac{\Lambda_{\pm}}{3} r_{\pm}^2. \quad (2)$$

Since the angular coordinates (θ, ϕ) are identified on the two-sphere, the corresponding angular coordinate basis vectors coincide on the hypersurface Σ .

¹ We are retaining explicit factors of G and c for clarity.

For the spherically symmetric thin shell, we adopt intrinsic coordinates $y^i = (c\tau, \theta, \phi)$, which are the same on both sides of the hypersurface, with τ the proper time measured by an observer at any point comoving with the shell. The isometric embedding into the 4D spacetime is given by $i_{\pm} : \Sigma \hookrightarrow \mathcal{M}$ and the functions

$$i_{\pm}^{\mu}(y^i) = x_{\pm}^{\mu}(y^i) = (ct_{\pm}(\tau), R_{\pm}(\tau), \theta, \phi),$$

with $R_{\pm}(\tau)$ denoting the comoving radius of the shell in each coordinate system. For a point with fixed angular coordinates (θ, ϕ) , the four-velocity is

$$u_{\pm}^{\mu} = c\dot{t}_{\pm} \delta_t^{\mu} + \dot{R}_{\pm} \delta_r^{\mu}, \quad (3)$$

where dots denote derivatives with respect to τ . The normalization condition $u^{\mu}u_{\mu} = c^2$ yields

$$\mathbf{u}_{\pm} = \left(c \frac{\sqrt{f_{\pm} + \dot{R}_{\pm}^2}}{f_{\pm}}, \dot{R}_{\pm}, 0, 0 \right). \quad (4)$$

The four-velocity can be related to a 3-vector \mathbf{v} if the 3-vector at a point in Σ , with coordinates $y^i = (c\tau, \theta, \phi)$, is pushforwarded to \mathcal{M} , where the coordinates are $x_{\pm}^{\mu}(\tau) = (ct_{\pm}(\tau), R_{\pm}(\tau), \theta, \phi)$. By defining

$$\mathbf{u}_{\pm} \equiv i_{\pm}^{\pm}(\mathbf{v}) = v^i \frac{\partial x_{\pm}^{\mu}}{\partial y^i} \partial_{\mu}^{\pm}, \quad (5)$$

we obtain the four-velocity in \mathcal{M} . Note that y^i ($i = 1, 2, 3$) denote coordinates intrinsic to the hypersurface Σ , and x_{\pm}^{μ} the coordinates on the bulk manifold \mathcal{M} . The induced metric (or first fundamental form) h_{ij}^{\pm} on Σ is obtained via the pull-back of the metric tensor $g_{\mu\nu}^{\pm}$:

$$h_{ij}^{\pm} \equiv [(i^{\pm})^* g^{\pm}]_{ij} = \frac{\partial x_{\pm}^{\alpha}}{\partial y^i} \frac{\partial x_{\pm}^{\beta}}{\partial y^j} g_{\alpha\beta}^{\pm}. \quad (6)$$

In the context of junction conditions [10, 12, 13] in general relativity, the continuity of the first fundamental form across the thin shell Σ requires that the induced metric computed from the interior geometry (\mathcal{M}^-) matches that computed from the exterior geometry (\mathcal{M}^+) at Σ :

$$h_{ij}^- = h_{ij}^+ \implies R_+ = R_- \equiv R \quad (7)$$

Although $r_+ = r_- = R$ on the hypersurface Σ , the radial coordinate basis vectors $\partial_{r_{\pm}}$ need not coincide there (see also [76]). The shell defines a timelike hypersurface (codimension one) Σ embedded in spacetime. The induced line element on Σ takes the form

$$ds_{\Sigma}^2 = h_{ij} dy^i dy^j = c^2 d\tau^2 - R(\tau)^2 (d\theta^2 + \sin^2 \theta d\phi^2). \quad (8)$$

Here, τ is the proper time of a comoving observer on the shell, and $R(\tau)$ is the comoving radius of the shell as a

function of τ . Moreover, since the four-velocity satisfies $u_{\pm}^{\mu} u_{\pm \mu}^{\nu} = c^2$, we obtain

$$c^2 = u_{\pm}^{\mu} u_{\pm \mu}^{\nu} = \left(v^i \frac{\partial x_{\pm}^{\mu}}{\partial y^i} \right) \left(v^j \frac{\partial x_{\pm}^{\nu}}{\partial y^j} \right) g_{\mu\nu}^{\pm} = v^i v^j h_{ij}^{\pm}. \quad (9)$$

Hence, at a point on the shell, a comoving observer with $v^{\theta} = v^{\phi} = 0$ has $v^{\tau} = c$.

The shell is modeled as an infinitesimally thin layer of matter-energy localized on Σ , where the intrinsic stress-energy tensor of the shell is defined as

$$S_{ij} = (\sigma + p/c^2) v_i v_j - p h_{ij}, \quad (10)$$

where σ is the surface energy density, p the surface pressure, v the shell 3-velocity, and h_{ij} the first fundamental form on the shell. The Levi-Civita connection $\hat{\nabla}$ on the shell is determined by the induced metric h_{ij} . Conservation of the shell stress-energy tensor S^{ij} is expressed as

$$\hat{\nabla}_i S^{ij} = \frac{1}{\sqrt{|h|}} \partial_i \left(\sqrt{|h|} S^{ij} \right) + \hat{\Gamma}^j_{ik} S^{ik} = 0. \quad (11)$$

Selecting the $j = \tau$ component gives

$$\frac{1}{\sqrt{|h|}} \partial_{\tau} \left(\sqrt{|h|} S^{\tau\tau} \right) + \hat{\Gamma}^{\tau}_{\theta\theta} S^{\theta\theta} + \hat{\Gamma}^{\tau}_{\phi\phi} S^{\phi\phi} = 0, \quad (12)$$

where $\sqrt{|h|} = R^2(\tau) \sin \theta$. The nonvanishing Christoffel symbols with an upper τ index are $\hat{\Gamma}^{\tau}_{\theta\theta} = R\dot{R}$ and $\hat{\Gamma}^{\tau}_{\phi\phi} = R\dot{R} \sin^2 \theta$. Therefore, Eq. (12) implies (see also [21])

$$\dot{\sigma} + \frac{2\dot{R}}{R} (\sigma + p/c^2) = 0. \quad (13)$$

The unit normal vector n_{\pm}^{μ} satisfies

$$u_{\pm}^{\mu} n_{\mu}^{\pm} = 0, \quad \epsilon \equiv n_{\pm}^{\mu} n_{\mu}^{\pm} = -1. \quad (14)$$

Since the hypersurface is timelike, its unit normal vector n_{\pm}^{μ} is spacelike and is chosen to point "outward" (i.e. toward increasing comoving radius) from the shell into the corresponding region. Solving the conditions in Eq. (14) yields

$$\mathbf{n}_{\pm} = \left(\frac{\dot{R}}{cf_{\pm}}, \sqrt{f_{\pm} + (\dot{R}/c)^2}, 0, 0 \right). \quad (15)$$

The extrinsic curvature as an object defined in Σ is written as (see Appendix A)

$$\mathcal{K}_{ij}^{\pm} = \frac{\partial x_{\pm}^{\mu}}{\partial y^i} \frac{\partial x_{\pm}^{\nu}}{\partial y^j} \nabla_{\mu} n_{\nu}^{\pm}. \quad (16)$$

The induced extrinsic curvature on the two sides by \mathcal{K}_{ij}^{\pm} , where the superscript \pm indicates evaluation using the normal n_{\pm}^{μ} and the metric function $f_{\pm}(r_{\pm})$ appropriate to the corresponding region.

The Israel junction conditions relate the jump in extrinsic curvature to the shell stress-energy [13]:

$$[\mathcal{K}_{ij}]_{\pm} = -\epsilon \frac{8\pi G}{c^4} \left(S_{ij} - \frac{1}{2} h_{ij} S \right), \quad (17)$$

where $[X]_{\pm} = X^+ - X^-$ denotes the difference between the outer (+) and inner (-) sides of the shell.

Considering the $\theta\theta$ components of the extrinsic curvature, we have

$$\mathcal{K}_{\theta\theta}^{\pm} = -\Gamma_{\theta\theta}^{\mu} n_{\mu}^{\pm} = f_{\pm}^{-1} \Gamma_{\theta\theta}^r n_{\pm}^r = -R \sqrt{f_{\pm} + (\dot{R}/c)^2}.$$

Using Eq. (17), this yields the junction condition for the timelike hypersurface Σ ($\epsilon = -1$):

$$\sqrt{f_- + (\dot{R}/c)^2} - \sqrt{f_+ + (\dot{R}/c)^2} = \frac{4\pi G}{c^2} \sigma(R) R. \quad (18)$$

By spherical symmetry, the $\phi\phi$ -component of the induced extrinsic curvature does not provide any additional information. Note that differentiating Eq. (18) with respect to the proper time τ and using also the energy conservation equation for the shell (Eq. (13)) yields the same equation as obtained from the $[\mathcal{K}_{\tau\tau}]_{\pm}$ component for the radial acceleration

$$\left[\frac{\frac{Gm}{R^2} - \frac{c^2 \Lambda R}{3} + \ddot{R}}{c^2 \sqrt{f + \dot{R}^2/c^2}} \right]_{\pm} = \frac{4\pi G}{c^2} (\sigma + 2p/c^2). \quad (19)$$

A. Linear equation of state

Before constructing static shell solutions, we note that the adiabatic sound speed along a surface layer with energy density σ and pressure $p = p(\sigma)$ is

$$c_s^2 = \frac{dp}{d\sigma}. \quad (20)$$

For $p = w\sigma c^2$ with constant w , one has $c_s^2 = wc^2$. If $w < 0$, this gives $c_s^2 < 0$ (imaginary sound speed) and a gradient instability. This can be avoided by allowing a more general linear response of p to σ .

Consider a linear equation of state of the form

$$p = \lambda(\sigma - \sigma_1)c^2, \quad w(\sigma) \equiv \lambda \frac{\sigma - \sigma_1}{\sigma}, \quad (21)$$

where p is the pressure, σ the surface energy density, λ a constant, σ_1 a constant reference density. The square of the sound speed is given by $c_s^2 = \lambda c^2$, with the parameter λ satisfying $0 \leq \lambda \leq 1$. Substituting Eq. (21) into the energy conservation equation (13) and integrating yields the solution for the surface density as a function of the shell radius R :

$$\sigma(R) = \frac{\lambda\sigma_1}{1+\lambda} + C R^{-2(1+\lambda)} = \frac{\lambda\sigma_1}{1+\lambda} + D \left(\frac{R_0}{R} \right)^{2(1+\lambda)}, \quad (22)$$

with C being an integration constant, and we have defined as $D \equiv C R_0^{-2(\lambda+1)}$. For a shell, the previous expression Eq. (22) may be recast in the form

$$\sigma(R) = \frac{\sigma_0}{1+\lambda} \left[\lambda - w_0 + (1+w_0) \left(\frac{R_0}{R} \right)^{2(\lambda+1)} \right], \quad (23)$$

where σ_0 is the surface energy density of the shell at the radius R_0 , and w_0 denotes the equation-of-state parameter at R_0 . Note that

$$D = \frac{1+w_0}{1+\lambda} \sigma_0, \quad \sigma_1 = \frac{\lambda - w_0}{\lambda} \sigma_0.$$

Correspondingly, the tangential pressure of the shell is expressed as

$$p(R) = \frac{c^2 \left[(w_0 - \lambda) + \left(\frac{R_0}{R} \right)^{2(\lambda+1)} (1+w_0)\lambda \right] \sigma_0}{(1+\lambda)} \quad (24)$$

If we set $\lambda = w_0$ in Eq. (23), we recover the standard equation of state $p(R) = w_0 \sigma(R) c^2$ at R_0 , and the surface density reduces to the familiar form (see for instance in [4])

$$\sigma(R) = \sigma_0 \left(\frac{R_0}{R} \right)^{2(1+w_0)}. \quad (25)$$

Furthermore, let R_0 be the equilibrium radius. By expanding Eq. (23) to first order, we obtain

$$\sigma = \sigma_0 - \frac{2(1+w_0)\sigma_0 \delta R}{R_0}, \quad p = c^2 w_0 \sigma_0 - \frac{2c^2 \lambda (1+w_0)\sigma_0 \delta R}{R_0}. \quad (26)$$

For a thin shell at equilibrium radius R_0 with surface density σ_0 and equation of state as given by Eq. (21), a small radial perturbation δR implies, from surface stress-energy conservation, the first-order variations $\delta\sigma = -2(1+w_0)\sigma_0(\delta R/R_0)$ and $\delta p = -2\lambda(1+w_0)\sigma_0 c^2(\delta R/R_0)$, where $0 < \lambda \leq 1$ characterizes the linear pressure response. For negative-pressure shells with $-1 < w_0 < 0$, an outward perturbation lowers σ and makes the pressure more negative (increasing the tension), which tends to pull the shell back, while an inward perturbation raises σ and weakens the tension. Shells with positive pressure ($w_0 > 0$) behave similarly: contraction increases both σ and p , and expansion decreases them, providing a restoring response that can be tuned by the shell radius. By contrast, for phantom matter ($w_0 < -1$), expansion increases σ and reduces the magnitude of the tension, while contraction decreases σ and strengthens the tension, a response that generally amplifies perturbations and is therefore destabilizing for $\lambda > 0$. In the special case $\lambda = w_0$, the perturbations satisfy $\delta p \sim w_0(1+w_0)$ in particular, in the $w_0 < 0$ regime this choice effectively interchanges the stabilizing and destabilizing responses (due to tension) between the range $-1 < w_0 < 0$ and the phantom range $w_0 < -1$.

B. Equilibrium state and numerical analysis

Here, we rewrite the junction condition given in Eq. (18) in a more convenient form [15]:

$$\beta_- - \beta_+ = \kappa(R), \quad (27)$$

where we define

$$\beta_{\pm} \equiv \sqrt{f^{\pm} + (\dot{R}/c)^2}, \quad (28)$$

and

$$\kappa(R) \equiv \frac{4\pi G}{c^2} \sigma(R) R. \quad (29)$$

By factorizing $\beta_-^2 - \beta_+^2 = f_-(R) - f_+(R)$ and using the junction condition Eq. (27), we obtain

$$\beta_+ = \frac{f^- - f^+}{2\kappa} - \frac{\kappa}{2}, \quad \beta_- = \frac{f^- - f^+}{2\kappa} + \frac{\kappa}{2}. \quad (30)$$

After some algebraic manipulation, the system can be recast into the form of an effective energy equation,

$$\frac{\dot{R}^2}{2} + V_{\text{eff}}(R) = 0, \quad (31)$$

where we define the effective gravitational potential as

$$V_{\text{eff}} = \frac{c^2}{4} \left\{ f_+ + f_- - \left[\frac{(f_- - f_+)^2}{2\kappa^2} + \frac{\kappa^2}{2} \right] \right\}. \quad (32)$$

Differentiating Eq. (31) with respect to the proper time τ yields the equation of motion

$$\ddot{R} + V'_{\text{eff}}(R) = 0, \quad (33)$$

where the prime denotes a derivative with respect to R .

The equilibrium configuration is obtained by combining Eqs. (31), (33), and (34), and by imposing the conditions $\dot{R} = \ddot{R} = 0$ at a constant radius R_0 . A static shell at radius R_0 (with $\dot{R} = 0$) corresponds to a stationary point of the potential, i.e. $V_{\text{eff}}(R_0) = 0$ and $V'_{\text{eff}}(R_0) = 0$. The shell is *stable* [21] against radial perturbations if, in addition (see Eq. (33)),

$$V''_{\text{eff}}(R_0) > 0.$$

The effective potential $V_{\text{eff}}(R)$, derived by substituting Eqs. (2), (29) and (23) into the Eq.(32), is given explicitly by:

$$\begin{aligned} \frac{V_{\text{eff}}(R)}{c^2} = \frac{1}{4} \left\{ 2 - \frac{2Gm_-}{c^2 R} - \frac{2Gm_+}{c^2 R} - \frac{R^2 \Lambda_-}{3} - \frac{R^2 \Lambda_+}{3} \right. \\ \left. - \frac{(1+\lambda)^2 [6G(m_- - m_+) + c^2 R^3 (\Lambda_- - \Lambda_+)]^2}{288G^2 \pi^2 \sigma_0^2 \left[R_0^2 \left(\frac{R_0}{R} \right)^{2\lambda} (1+w_0) + R^2 (\lambda - w_0) \right]^2} - \frac{8G^2 \pi^2 \sigma_0^2 R^2 \left[-w_0 + \left(\frac{R_0}{R} \right)^{2(1+\lambda)} (1+w_0) + \lambda \right]^2}{c^4 (1+\lambda)^2} \right\}. \end{aligned} \quad (34)$$

1. Static stable thin shell in the case where $\Lambda_+ = \Lambda_-$

A particularly physically realistic class of static and stable dark-fluid thin shells—relevant, at least, for a late-time accelerating universe—emerges in the case $\Lambda_+ = \Lambda_- \equiv \Lambda$, where the positive cosmological constant den-

sity satisfies $\rho_{\Lambda} = \rho_{\text{crit}}$ [86]. This corresponds to matching two Schwarzschild–de Sitter spacetimes with distinct mass parameters $m_+ \neq m_-$. Under these conditions, imposing $\sigma_0 > 0$ in Eq. (27) at R_0 implies $[m]_{\pm} > 0$. The system then simplifies to:

$$V_{\text{eff}}(R_0) = -\frac{G(m_- + m_+)}{2R_0} + \frac{1}{96} c^2 \left(48 - 16R_0^2 \Lambda - \frac{3(m_- - m_+)^2}{\pi^2 R_0^4 \sigma_0^2} \right) - \frac{2G^2 \pi^2 R_0^2 \sigma_0^2}{c^2} = 0, \quad (35)$$

$$V'_{\text{eff}}(R_0) = \frac{G(m_- + m_+)}{2R_0^2} - \frac{1}{3} c^2 R_0 \Lambda - \frac{c^2 (m_- - m_+)^2 w_0}{8\pi^2 R_0^5 \sigma_0^2} + \frac{4G^2 \pi^2 R_0 (1 + 2w_0) \sigma_0^2}{c^2} = 0. \quad (36)$$

We use the above algebraic system of equations to identify the viable equilibrium configurations (R_0, σ_0) for

a given set of parameters $(m_{\pm}, \Lambda, \lambda, w_0)$. The second derivative of the effective potential evaluated at R_0 is given by:

$$V''_{\text{eff}}(R_0) = -\frac{G(m_- + m_+)}{R_0^3} + \frac{c^2}{24} \left[-8\Lambda - \frac{3(m_- - m_+)^2 (w_0(1 + 6w_0) - 2(1 + w_0)\lambda)}{\pi^2 R_0^6 \sigma_0^2} \right] - \frac{4G^2 \pi^2 (3 + 6w_0 + 4w_0^2 + 4(1 + w_0)\lambda) \sigma_0^2}{c^2} \quad (37)$$

Here, for a black hole with mass $m_- = 10^{10} M_{\odot}$, we numerically demonstrate that static and stable solutions exist in the range $-\frac{3}{7} \lesssim w_0 < \frac{1}{2}$ (see Fig.1). Shells with positive pressure are situated near the photon sphere, whereas negative values of w_0 drive the shell smoothly

toward the cosmological horizon.

2. Static stable thin shell in the case where $\Lambda_+ \neq \Lambda_-$

In the more general case with distinct cosmological constants ($\Lambda_+ \neq \Lambda_-$), the system of equations to be solved becomes:

$$V_{\text{eff}}(R_0) = -\frac{G(m_- + m_+)}{2R_0} - \frac{c^2}{12} (-6 + R_0^2(\Lambda_- + \Lambda_+)) - \frac{(6cG(m_- - m_+) + c^3 R_0^3(\Lambda_- - \Lambda_+))^2}{1152 G^2 \pi^2 R_0^4 \sigma_0^2} - \frac{2G^2 \pi^2 R_0^2 \sigma_0^2}{c^2} = 0 \quad (38)$$

$$V'_{\text{eff}}(R_0) = -\frac{1}{576 c^2 G^2 \pi^2 R_0^5 \sigma_0^2} \left[6c^6 G(m_- - m_+) R_0^3 (3 + 4w_0)(\Lambda_- - \Lambda_+) + c^8 R_0^6 (3 + 2w_0)(\Lambda_- - \Lambda_+)^2 - \right. \quad (39)$$

$$\left. -288c^2 G^3 (m_- + m_+) \pi^2 R_0^3 \sigma_0^2 - 2304G^4 \pi^4 R_0^6 (1 + 2w_0) \sigma_0^4 + 24c^4 G^2 (3(m_- - m_+)^2 w_0 + 4\pi^2 R_0^6 (\Lambda_- + \Lambda_+) \sigma_0^2) \right] = 0$$

Stability of the shell under radial perturbations requires

$$V''_{\text{eff}}|_{R_0} > 0,$$

where the second derivative of the effective potential at R_0 is given by:

$$V''_{\text{eff}}(R_0) = -\frac{G(m_- + m_+)}{R_0^3} + \frac{c^2}{24} \left[-4(\Lambda_- + \Lambda_+) - \frac{3(m_- - m_+)^2 (w_0(1 + 6w_0) - 2(1 + w_0)\lambda)}{\pi^2 R_0^6 \sigma_0^2} \right] - \frac{c^6 (15 + 26w_0 + 12w_0^2 - 4(1 + w_0)\lambda)(\Lambda_- - \Lambda_+)^2}{576 G^2 \pi^2 \sigma_0^2} + \frac{c^4 (m_- - m_+) [3 + 2w_0(7 + 6w_0 - 2\lambda) - 4\lambda] (-\Lambda_- + \Lambda_+)}{48 G \pi^2 R_0^3 \sigma_0^2} - \frac{4G^2 \pi^2 (3 + 6w_0 + 4w_0^2 + 4(1 + w_0)\lambda) \sigma_0^2}{c^2} \quad (40)$$

Our next objective is to identify the viable equilibrium configurations (R_0, σ_0) for a given parameter set

$(m_{\pm}, \Lambda_{\pm}, \lambda, w_0)$. This is accomplished by solving the coupled system defined by Eqs. (38) and (39). Subsequently,

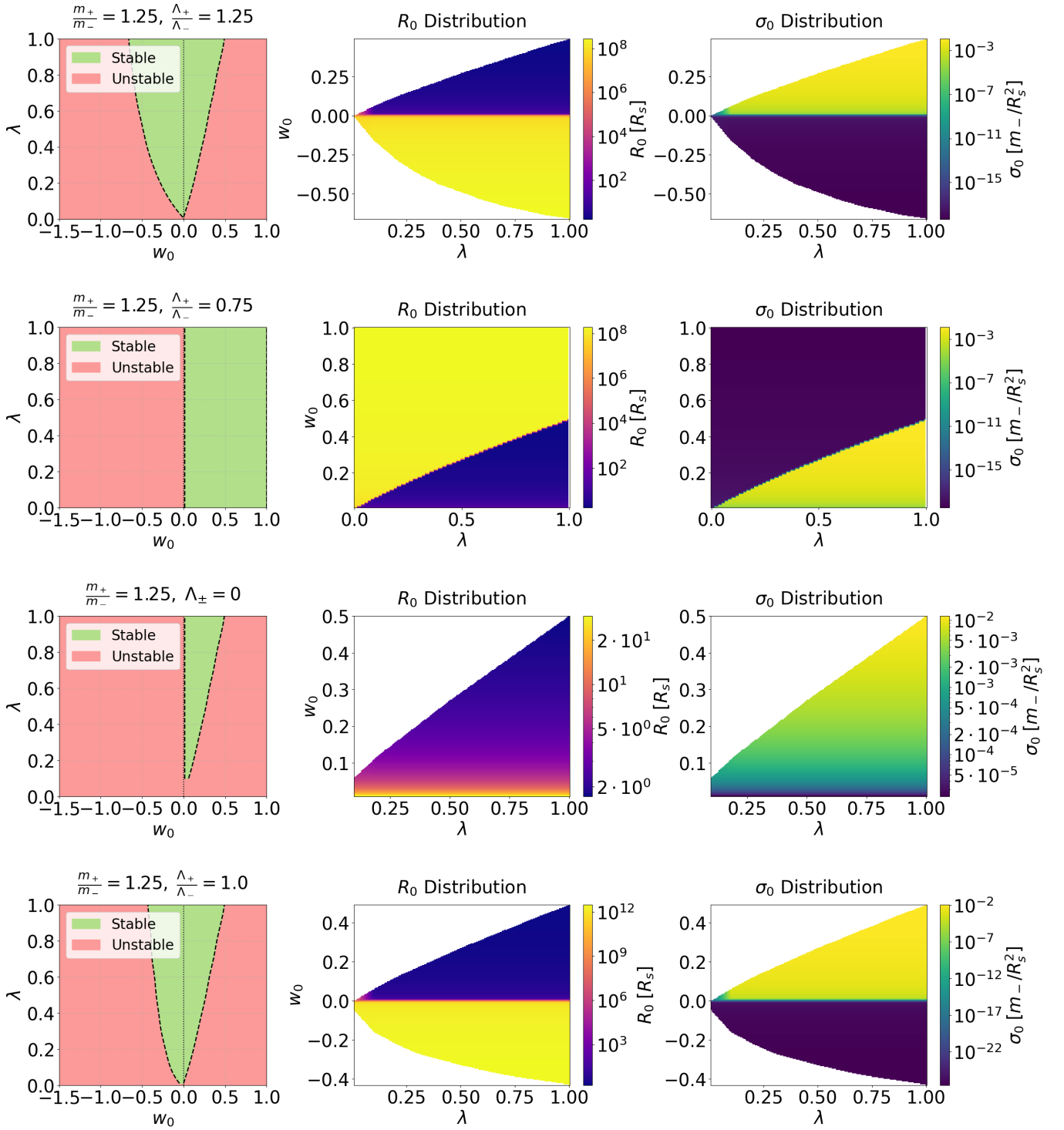


FIG. 1: We set $m_- = 10^{10} M_\odot$ and consider a cosmological-constant-dominated universe with $\rho_{\Lambda_+} = \rho_{\text{crit}} = 3H_0^2/(8\pi G)$ [86].

We numerically solve for (R_0, σ_0) the system of Eqs. (38) and (39) while requiring that Eq. (40) be positive and that condition Eq. (41) be satisfied and we plot the stability regions in the (w_0, λ) parameter space (left column), together with the corresponding equilibrium radius R_0 distribution over the stable region (middle column), and the surface energy density σ_0 distribution (right column) for each (w_0, λ) in the stable domain. The rows correspond to the cases: (a)

$m_+/m_- = \Lambda_+/\Lambda_- = 1.25$, (b) $m_+/m_- = 1.25, \Lambda_+/\Lambda_- = 0.75$, (c) $m_+/m_- = 1.25, \Lambda_\pm = 0$, and (d) $m_+/m_- = 1.25, \Lambda_+/\Lambda_- = 1.0$. The colorbars represent the equilibrium radius in units of the Schwarzschild radius (R_s) and the surface density in units of the characteristic scale m_-/R_s^2 . The reddish or white areas in the distribution plots indicate regions where either (i) no static equilibrium with $\sigma_0 > 0$ exists, or (ii) a static equilibrium exists but is unstable ($V''_{\text{eff}}(R_0) < 0$).

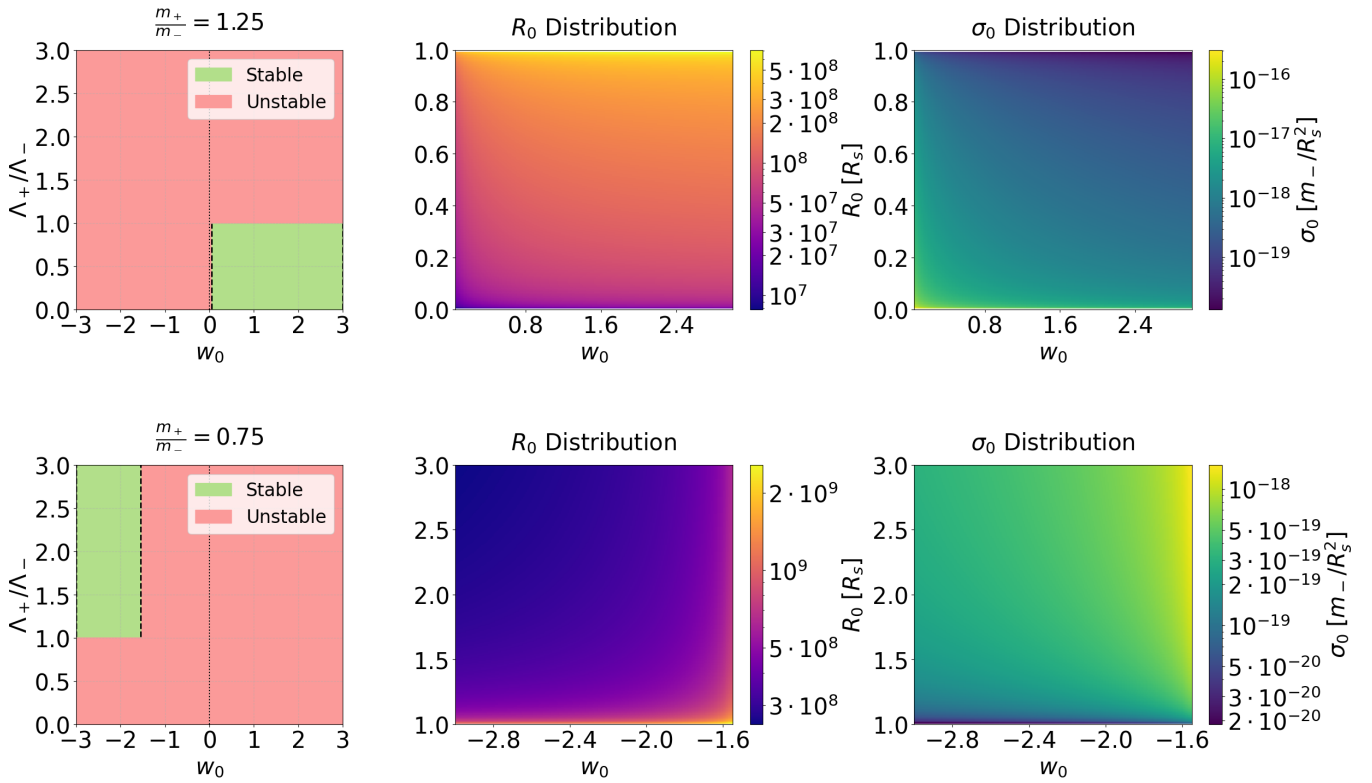


FIG. 2: We set $m_- = 10^{10} M_\odot$ and consider a cosmological-constant-dominated universe with $\rho_{\Lambda_+} = \rho_{\text{crit}} = 3H_0^2/(8\pi G)$ [86]. By imposing $w_0 = \lambda$, i.e., assuming Eq. (25), we numerically solve the system of Eqs. (38) and (39) for (R_0, σ_0) . In doing so, we require that Eq. (40) be positive and that the condition in Eq. (41) be satisfied. We then plot the stability regions in the $(w_0, \Lambda_+/\Lambda_-)$ parameter space (left column), together with the corresponding equilibrium radius R_0 distribution over the stable region (middle column), and the surface energy density σ_0 distribution (right column) for each $(w_0, \Lambda_+/\Lambda_-)$ within the stable domain. The top row corresponds to the mass ratio $m_+/m_- = 1.25$, while the bottom row corresponds to $m_+/m_- = 0.75$. **Left column:** Stability regions in the parameter space spanned by the equation-of-state parameter w_0 and the cosmological constant ratio Λ_+/Λ_- . Green areas represent stable configurations ($V''_{\text{eff}} > 0$), whereas red areas indicate instability. **Middle and right columns:** Distributions of the normalized equilibrium radius R_0 (measured in units of the Schwarzschild radius R_s) and the surface energy density σ_0 , respectively. The heatmaps are shown only for configurations that satisfy the stability conditions.

the stability of each identified equilibrium is assessed by evaluating the sign of the second derivative of the effective potential, as given by Eq. (40), requiring $V''_{\text{eff}}(R_0) > 0$ for stability. We assume that the surface energy density of the shell is positive at R_0 , i.e. $\sigma_0 > 0$. Accordingly, we will only accept solutions for which the following condition holds:

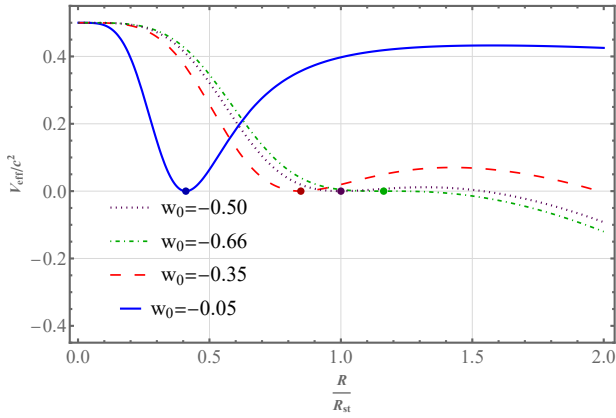
$$-\frac{2G}{c^2 R_0} [m]_{\pm} < \frac{R_0^2}{3} [\Lambda]_{\pm}. \quad (41)$$

$$\frac{m_+}{m_-} > 1, \quad \frac{\Lambda_+}{\Lambda_-} > 1; \quad \frac{m_+}{m_-} > 1, \quad \frac{\Lambda_+}{\Lambda_-} = 1; \quad \frac{m_+}{m_-} > 1, \quad \frac{\Lambda_+}{\Lambda_-} < 1,$$

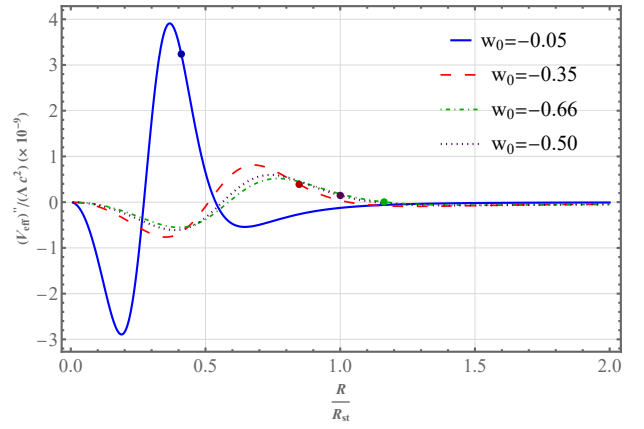
As shown in Figs. 1–2, both the existence and the size of the stability region in the w_0 – λ parameter space (for $\sigma_0 > 0$) depend sensitively on the relative values of the mass and cosmological constant ratios. Throughout this work, we fix $m_- = 10^{10} M_\odot$. In Fig. 1, we numerically solve for (R_0, σ_0) the system of Eqs. (38) and (39) while requiring that Eq. (40) be positive and that condition Eq. (41) be satisfied. We find that the only static stable thin shells occur in the following cases²:

² Static stable configurations satisfying $m_+/m_- < 1$ exist but

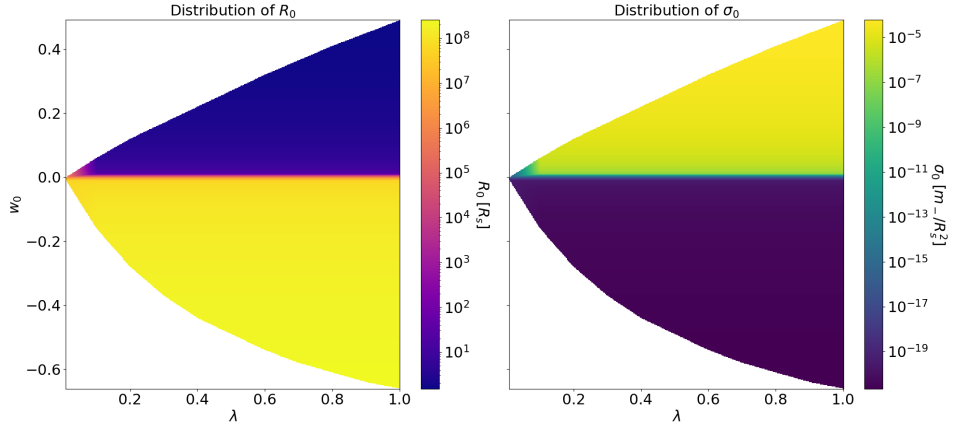
require $\lambda < 0$, which leads to instability through an imaginary



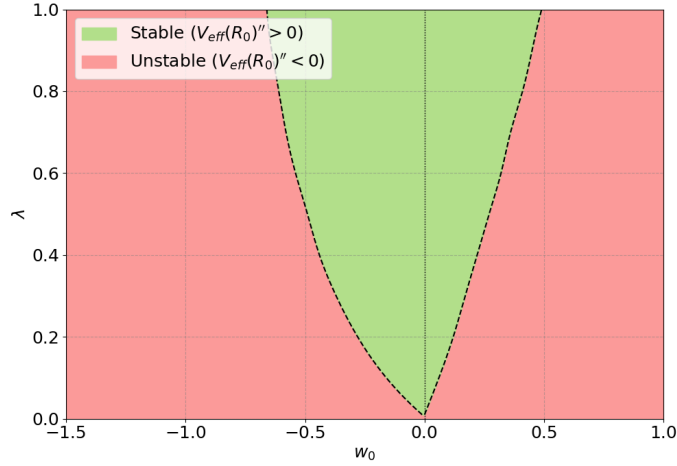
(a) We present a plot of V_{eff}/c^2 as a function of R/R_{st} , where $R_{\text{st}} \equiv \left[\frac{3Gm_-}{\Lambda c^2} \right]^{1/3}$, $\Lambda \equiv (\Lambda_+ + \Lambda_-)/2$, when $\lambda = 1$. The effective potential, defined in Eq. (32), plotted for shell parameters corresponding to equilibrium at R_0 . Positive values, $V_{\text{eff}} > 0$, represent energetically forbidden regions, since Eq. (31) would require $\dot{R}^2 < 0$.



(b) We present a plot of $\frac{V_{\text{eff}}''}{\Lambda c^2} (\times 10^{-9})$, where $\Lambda \equiv (\Lambda_+ + \Lambda_-)/2$, as a function of R/R_{st} , where $R_{\text{st}} \equiv \left[\frac{3Gm_-}{\Lambda c^2} \right]^{1/3}$, when $\lambda = 1$. Stability is ensured by a local minimum of the effective potential at R_0 , with $V_{\text{eff}}''(R_0) > 0$.



(c)



(d)

FIG. 3: We set $m_- = 10^{10} M_\odot$ in a cosmological-constant-dominated universe with $\rho_{\Lambda_+} = \rho_{\text{crit}} = 3H_0^2/(8\pi G)$ [86], and consider parameters satisfying $m_+/m_- = \Lambda_+/\Lambda_- = 1.001$. The static radius in the corresponding SdS spacetimes is $R_{\text{st}} \simeq 6.52 \times 10^{21}$ m, defined as $R_{\text{st}} \equiv \left[\frac{3Gm_-}{\Lambda c^2} \right]^{1/3}$ with $\Lambda = (\Lambda_+ + \Lambda_-)/2$. For $-2/3 < w_0 < 0$, stable static shells exist near R_{st} , with $w_0 = -2/3$ marking the stability boundary when $\lambda = 1$. In the narrower range $0.01 \lesssim w_0 < 0.5$, the stable radii cluster around $R \sim 10^{13-14}$ m, approaching the photon sphere $3Gm_-/c^2 \simeq 4.43 \times 10^{13}$ m at $w_0 = 0.5$ (but always exceeding it[15]). This illustrates how the stability region depends on $m_+/m_- > 1$ and $\Lambda_+/\Lambda_- > 1$.

as well as the special case of matched Schwarzschild metrics,

$$\frac{m_+}{m_-} > 1, \quad \Lambda_+ = \Lambda_- = 0.$$

In any case, stability is lost when $\lambda = w_0 = 0$. Furthermore, the overall shape of the stability region in the w_0 - λ plane is largely insensitive to the specific numerical values of the mass and cosmological-constant ratios, depending only on whether these ratios are greater than, less than, or equal to unity. Variations in these ratios instead modify the equilibrium quantities σ_0 and R_0 , as illustrated in Fig. 1.

An additional regime of stability arises when $\lambda = w_0$ (see Eq.(25)). In this case, stable configurations are found approximately for $0 \lesssim w_0 \lesssim 1$, and may occur when the mass ratio satisfies $m_+/m_- > 1$ and $\Lambda_+/\Lambda_- < 1$, or when $m_+/m_- < 1$ and $\Lambda_+/\Lambda_- > 1$, and for $w_0 \lesssim -1.5$ (see Fig. 2). However, within this regime, shells with $w_0 < 0$ can become unstable if the squared sound speed becomes negative, $c_s^2 < 0$ [85]. The physically relevant solutions correspond to the case $\Lambda_+/\Lambda_- < 1$ with $0 \lesssim w_0 \lesssim 1$, where the stable radii are tightly concentrated around the static radius scale. Since this regime is already contained within the broader case where $w_0 \neq \lambda$, it does not introduce new qualitative features, and we therefore do not perform an extended analysis for it.

The presence of a cosmological constant therefore allows for static stable shells to exist at multiple characteristic scales, which may be naturally classified as configurations near the black hole, near the cosmological horizon, or near the static radius scale $R_{\text{st}} \equiv \left[\frac{3Gm_-}{\Lambda c^2} \right]^{1/3}$, $\Lambda \equiv (\Lambda_+ + \Lambda_-)/2$. It should be emphasized that R_{st} here denotes only a characteristic scale and does not retain its usual interpretation as the static radius in Schwarzschild-de Sitter spacetime (see Appendix B). The coupling between the mass and cosmological-constant ratios becomes most pronounced when the equilibrium radius satisfies $R_0 \sim R_{\text{st}}$. This situation also arises for negative-pressure shells when $\Lambda_+/\Lambda_- > 1$ and $m_+/m_- > 1$, as well as for positive-pressure shells in the case $\Lambda_+/\Lambda_- < 1$ with $m_+/m_- > 1$. More generally, static and stable shells forming near the black hole or near the cosmological horizon are highly insensitive to the specific values of the ratios Λ_+/Λ_- and m_+/m_- , respectively, as long as we remain within a given branch defined by the relation between Λ_+ and Λ_- (i.e., $\Lambda_+ > \Lambda_-$, $\Lambda_+ = \Lambda_-$, or $\Lambda_+ < \Lambda_-$), each of which yields distinct families of shell solutions. It is further evident that the case $\lambda = 1$ yields the widest allowed range of the equation-of-state parameter w_0 (see Fig. 3). Finally, static stable shells with positive surface energy density $\sigma_0 > 0$, negative pressure ($w_0 < 0$), and sound-speed parameter $\lambda > 0$ exist only when $m_+/m_- > 1$ and $\Lambda_+/\Lambda_- \geq 1$.

In Fig. 4 we illustrate the three cases. For $\Lambda_+ = \Lambda_-$ with $m_+ > m_-$, stability for $\lambda = 1$ is found in the range $-3/7 \lesssim w_0 \lesssim 1/2$. Static, stable shells with positive pressure are located near the photon sphere; as the pressure increases, the shells approach the photon sphere asymptotically but never coincide with it. As w_0 becomes negative, the shell radius moves rapidly but smoothly toward the cosmological horizon, approaching it more closely as the lower stability bound (higher tension) is reached. For $\Lambda_+ > \Lambda_-$, static stable thin shells of $\lambda = 1$ exist approximately in the interval $-2/3 \lesssim w_0 \lesssim 1/2$. Positive-pressure configurations are again mainly located near the photon sphere and behave similarly to the previous case. However, at $w_0 = 0$ the transition is smooth: as w_0 becomes more negative, negative-pressure shells appear and extend outward only up to the scale of the static radius, rather than reaching the cosmological horizon. Finally, for $\Lambda_+ < \Lambda_-$, static stable shells of $\lambda = 1$ are found in the range $0 \leq w_0 \leq 1$. Shells with $0 < w_0 < 1/2$ lie near the photon sphere, and around $w_0 = 1/2$ the configuration undergoes a rapid but smooth transition toward scales determined by the static radius.

Intuitively, note that the equation of state parameter is defined as $w \equiv w(\sigma)$. As the surface energy density $\sigma(R)$ varies around R_0 within the range of parameters for which $\lambda > 0$ and stability is ensured through $p(R)$, the equation of state parameter $w(\sigma)$ may change sign appropriately. This allows stability to be achieved by combining the effects of negative and positive pressure. For negative-pressure shells at R_0 , an outward radial perturbation reduces σ , leading to a more negative pressure (i.e., increased tension), which then pulls the shell back inward. Conversely, an inward perturbation increases σ , weakening the tension. Consequently, such shells must reside in a region of repulsive gravity to maintain equilibrium, or in a region of sufficiently weak attractive gravity such that an inward perturbation causes $w(\sigma)$ to increase rapidly enough (becoming sufficiently positive) to counteract the gravitational pull on the shell. For positive-pressure shells at R_0 , the behavior is analogous: contraction increases both σ and p , producing a restoring response, while expansion decreases them. In this case, equilibrium requires either a region of attractive gravity, or a region of sufficiently weak repulsive gravity such that an outward perturbation causes $w(\sigma)$ to decrease rapidly enough (becoming sufficiently negative) to counteract the repulsive effect experienced by the shell.

III. LINEAR PERTURBATIONS AND DYNAMICAL EVOLUTION

Several astrophysical mechanisms can perturb a static thin shell away from equilibrium. For example, accretion of infalling matter—energy may transfer radial momentum to the shell and increase its surface energy density [121]; mergers (i.e., changes in the central black hole mass) or close encounters can impulsively displace the

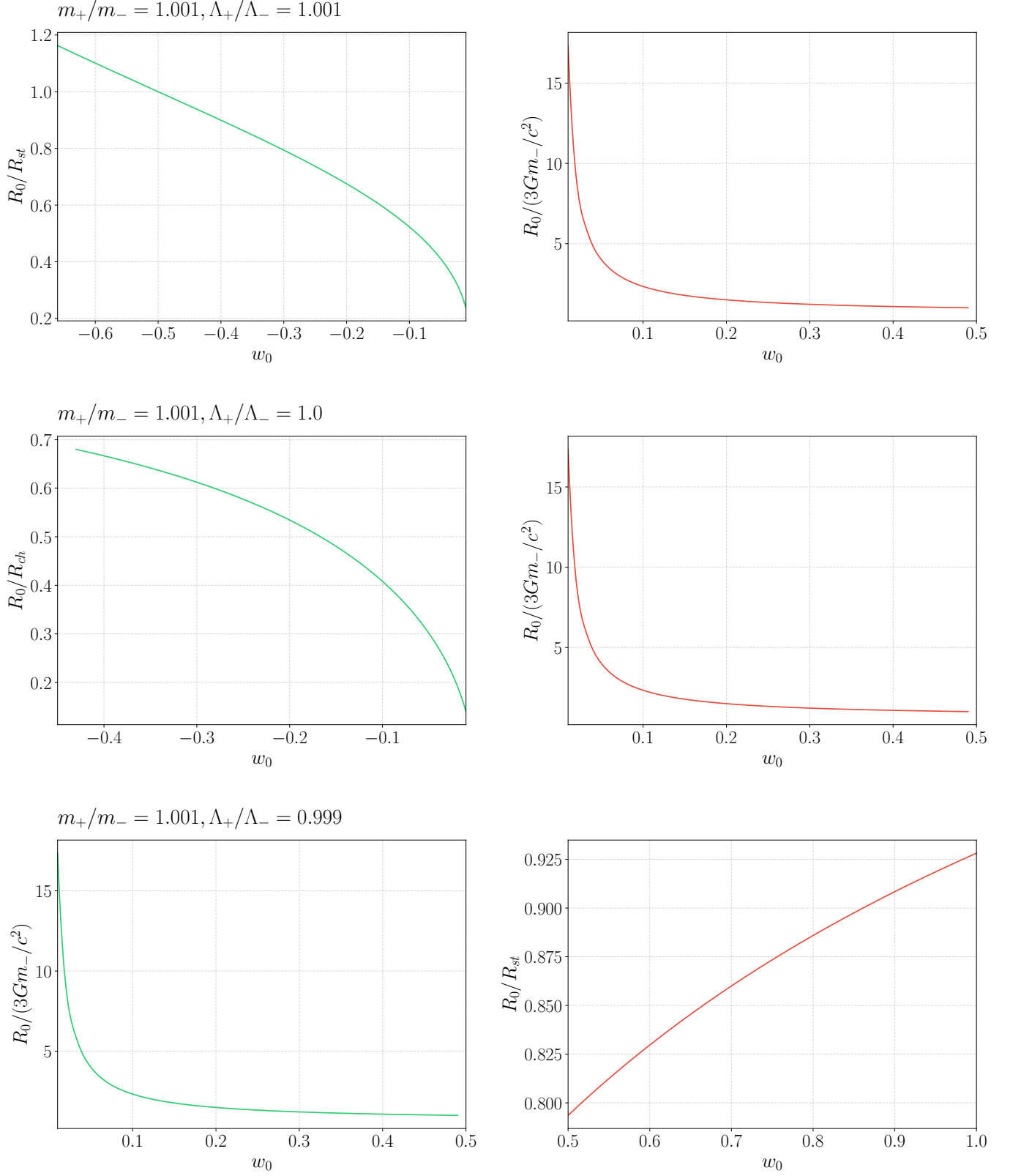


FIG. 4: Normalized stable shell radius R_0 as a function of the equation of state parameter w_0 for a fixed sound speed $\lambda = 1$. The figure displays three distinct mass-vacuum energy configurations. **Top Row (Case 1):** A slight mass and vacuum energy excess ($m_+/m_- = 1.001, \Lambda_+/\Lambda_- = 1.001$). The left panel shows the negative pressure branch ($w_0 < 0$) normalized to the static radius R_{st} , while the right panel shows the positive pressure branch ($w_0 > 0$) normalized to the photon ring radius $3Gm_-/c^2$. **Middle Row (Case 2):** A significant mass excess with equal vacuum energies ($m_+/m_- = 1.001, \Lambda_+/\Lambda_- = 1.0$). The left panel displays the negative pressure branch normalized to the cosmic horizon R_{ch} , and the right panel shows the positive pressure branch normalized to the photon ring. **Bottom Row (Case 3):** A mass excess coupled with a vacuum energy deficit ($m_+/m_- = 1.001, \Lambda_+/\Lambda_- = 0.999$). The left panel shows the small astrophysical branch stable for $0 < w_0 < 0.5$, while the right panel shows the large cosmological branch stable for $0.5 < w_0 < 1$.

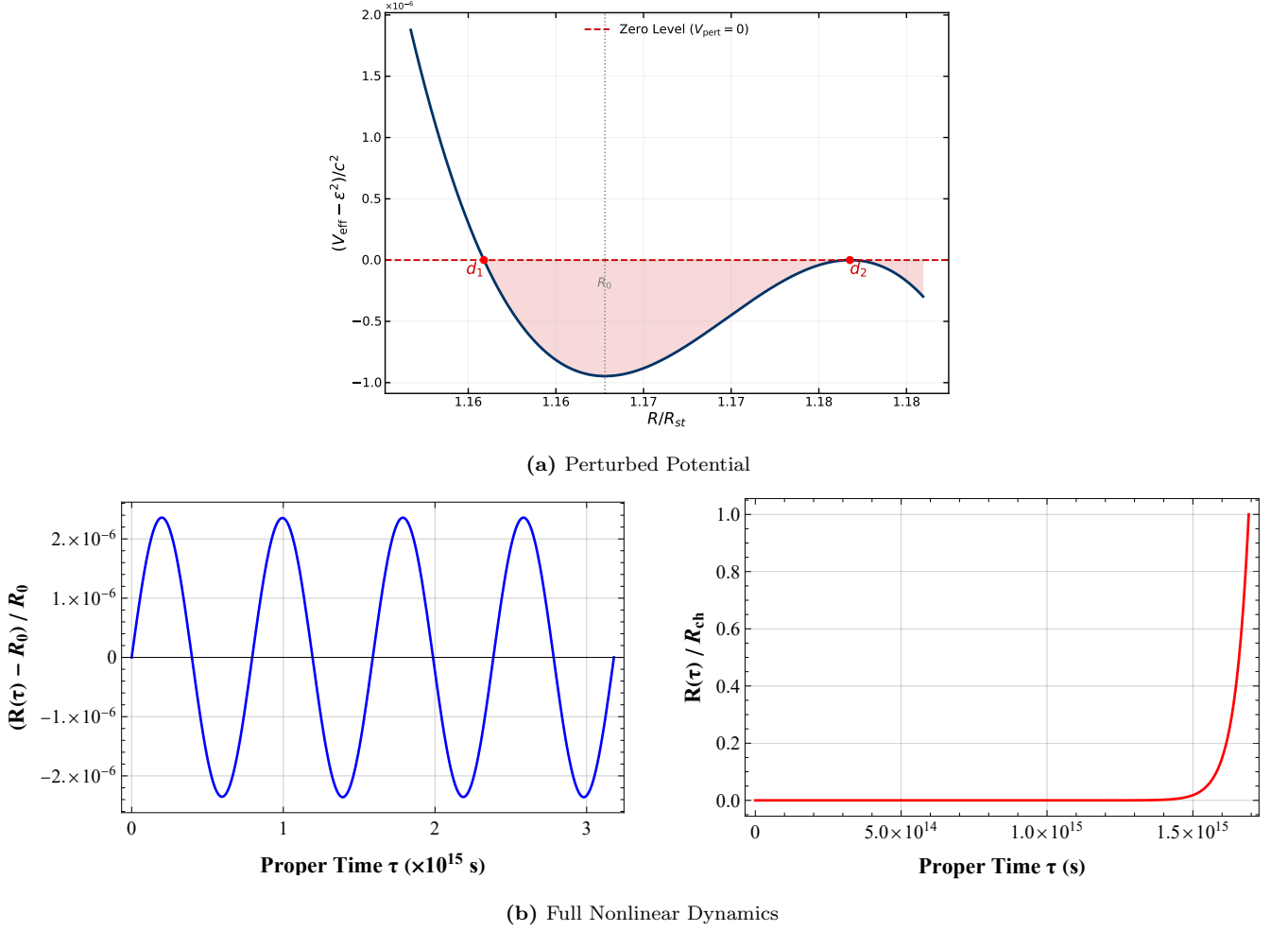


FIG. 5: Stability analysis of the shell for the case where $m_+/m_- = 1.001$ and $\Lambda_+/\Lambda_- = 1.001$. (a) The effective potential shifted by the perturbation energy, $(V_{\text{eff}}(R) - \epsilon^2)/c^2$. The shell is confined between the turning points d_1 and d_2 where the potential becomes negative. (b) Solutions to the exact equation of motion $\ddot{R} = -V'_{\text{eff}}(R)$. For initial velocities $\dot{R} < \sqrt{2}\epsilon_{\text{crit}}$ (blue, $\epsilon = 100$ m/s), the motion remains bounded (stable). Conversely, if $\dot{R} \geq \sqrt{2}\epsilon_{\text{crit}}$ (red, $\epsilon = 2.92715 \times 10^5$ m/s), the shell overcomes the potential barrier and escapes to cosmic horizon (unbounded instability).

shell from equilibrium. Interestingly, cosmological Hubble expansion can quasi-statically and slowly shift thin-shell equilibrium configurations away from their minima for shells located at scales of order $\sim R_{\text{st}}$ or larger. This process unfolds on a timescale $\sim H_0^{-1}$, which is quite longer than the characteristic oscillation period ($\sim 10^{15}$ s).

The radial dynamics can be written as the first-order system $\dot{R} = v$, $\dot{v} = -V'_{\text{eff}}(R)$, admitting the conserved energy $0 \equiv E = \frac{1}{2}v^2 + V_{\text{eff}}(R)$. The static shell is the equilibrium $(R_0, 0 = v_0 = \dot{R}|_{R=R_0})$ with $V_{\text{eff}}(R_0) = V'_{\text{eff}}(R_0) = 0$. If V_{eff} sufficiently differentiable near R_0 and $V''_{\text{eff}}(R_0) > 0$, then R_0 is a strict local minimum of V_{eff} and the zero-energy level is (locally) the isolated point $(R_0, 0)$. The energy E is therefore a Lyapunov function in a neighborhood of the equilibrium (but not a strict Lyapunov function since $\dot{E} \equiv 0$). Consequently

$(R_0, 0)$ is stable but not asymptotically stable [122].

A physically more relevant notion of stability is that of bounded excursion (see [21]). Here, the effective potential is perturbed by a constant shift so that the energy level is slightly raised; the formerly isolated equilibrium point $(R_0, 0)$ then becomes an interval between two turning points. Suppose we perturb $V_{\text{eff}} \rightarrow V_{\text{eff}} - \epsilon^2$, then there exist small positive numbers d_1 and d_2 such that the effective potential satisfies

$$V(R_0 - d_1) = 0, \quad V'(R_0 - d_1) \leq 0, \quad (42)$$

$$V(R_0 + d_2) = 0, \quad V'(R_0 + d_2) \geq 0$$

with $V(R) < 0$ for all R in the interval $(R_0 - d_1, R_0 + d_2)$. In particular, let $\delta R < \frac{d_1 + d_2}{2}$ then Eq. (31) at second order is written as

$$\delta \dot{R}^2 + V''(R_0)\delta R^2 = 2\epsilon^2, \quad (43)$$

where the prime denotes a derivative with respect to R . To determine the threshold between stable oscillations and unbounded motion, we calculate the critical perturbation parameter, ϵ_{crit} . This value corresponds to the energy required for the shell to overcome the potential barrier (the “hill”) adjacent to the stable equilibrium. Let R_{hill} denote the location of the unstable maximum of the effective potential. The critical velocity parameter is then given by the square root of the potential difference between the barrier top and the potential minimum:

$$\epsilon_{\text{crit}} = \sqrt{V_{\text{eff}}(R_{\text{hill}}) - V_{\text{eff}}(R_0)}. \quad (44)$$

If we now impose initial conditions compatible with Eq. (43)—specifically, starting at $R_{\text{init}} = R_0$ with an initial velocity $\dot{R}_{\text{init}} \ll \sqrt{2}\epsilon_{\text{crit}}$ —the ensuing motion described by Eq. (33) is oscillatory, and the assumption of no back-reaction remains well justified. In this regime, differentiating Eq. (43) with respect to τ yields the equation of motion of a simple harmonic oscillator:

$$\delta\ddot{R} + \omega^2\delta R = 0, \quad (45)$$

where the angular frequency of the oscillation is $\omega = \sqrt{V''_{\text{eff}}(R_0)}$.

The results of this numerical analysis are presented in Fig. 5. Figure 5(a) depicts the shape of the effective potential perturbed by a constant energy shift, illustrating the bounded region between turning points d_1 and d_2 . In Fig. 5(b), we show the time evolution of the shell radius $R(\tau)$ for two distinct initial velocity perturbations, starting from the equilibrium configuration $R_{\text{init}} = R_0$.

To validate the stability criteria derived from the effective potential, we numerically integrate the equation of motion for the shell, given by Eq. (33), for a specific configuration characterized by the equation of state parameter $w = -0.66$ and $\lambda = 1$. We introduce a slight asymmetry between the interior and exterior spacetime regions, defined by the mass and cosmological constant ratios $m_+/m_- = \Lambda_+/\Lambda_- = 1.001$ and further set $m_- = 10^{10} M_\odot$ and $\rho_{\Lambda_+} = \rho_{\text{crit}}$ [86]. For the chosen parameters, numerical evaluation yields a critical value of $\epsilon_{\text{crit}} \approx 2.91 \times 10^5$ m/s. Consequently, the period of these linear oscillations is given by $T = 2\pi/\omega$. For the system parameters described above, we find $T \approx 7.9 \times 10^{14}$ s.

First, we consider a small perturbation with $\epsilon = 100$ m/s. Since this value satisfies the condition $\dot{R}_{\text{init}} \ll \sqrt{2}\epsilon_{\text{crit}}$, consequently, the motion is confined to the potential valley, resulting in stable oscillations around R_0 , as shown by the blue curve. Second, we apply an initial velocity determined from $\epsilon = 2.92715 \times 10^5$ m/s. This value slightly exceeds the critical threshold $\epsilon_{\text{crit}} \approx 2.91 \times 10^5$ m/s. In this regime ($\dot{R}_{\text{init}} \geq \sqrt{2}\epsilon_{\text{crit}}$), the shell possesses sufficient energy to cross the unstable maximum (the “hill”) of the effective potential. Once over the barrier, the restoring force vanishes and becomes repulsive, driving the shell toward the cosmic horizon. This unbounded instability is depicted by the red curve in

Fig. 5(b). Although this energy is sufficient to induce back-reaction and deform the small stability valley, it remains negligible compared to the left uphill of the potential (see Fig. 3a), justifying the conclusion in this specific example that a shell with such a perturbation will reach the cosmic horizon rather than fall into the black hole. A similar analysis can be performed for shells with $w_0 > 0$ that are situated near the black hole and ultimately collapse into the black-hole horizon. A self-consistent perturbation analysis including back reaction would require the full linearised Einstein equations and is beyond the scope of the present work.

IV. OBSERVATIONAL SIGNATURES OF A STATIC STABLE DARK FLUID SHELL

Several works have explored the observational signatures of thin shells and shell-like structures surrounding black holes, gravastars, wormholes, focusing on their impact on strong-field gravitational lensing and on the detailed morphology of the black hole shadow and associated photon rings [72–79]. We assume a dark matter or dark energy shell, by its nature, does not interact electromagnetically and therefore cannot be observed directly via emission or absorption of photons. However, its gravitational influence alters both the propagation of light, leading to potential observational signatures [76]. Throughout this analysis, we assume the shell to be transparent.

While the present analysis relies on the assumption of a completely transparent dark fluid shell, relaxing this condition would fundamentally alter the predicted phenomenological signatures. If the shell possesses non-negligible opacity or electromagnetic interaction, the strictly geometric derivation of the shadow’s critical angular radius Θ_{crit} would be insufficient. An optically thick shell located outside the photon sphere would obscure the central black hole shadow, effectively replacing it with a localized absorption profile at the equilibrium radius R_0 . Conversely, if the shell matter emits or scatters radiation, it could introduce a secondary luminous ring or a diffuse halo that competes visually with the classic photon ring. In such non-transparent scenarios, detailed general relativistic radiative transfer (GRRT) calculations would be necessary to disentangle the shell’s intrinsic emission or absorption features from the purely refractive gravitational magnification discussed here.

Consider the case without a shell, i.e., a pure SdS spacetime with mass parameter $m = m_-$ and the cosmological constant Λ set to its Planck value [86]. In this scenario, we have (see Appendix B)

$$\sin^2\theta_{\text{crit}} = \frac{f(r_O)b_{\text{crit}}^2}{r_O^2}, \quad (46)$$

where r_O denotes the radial coordinate of the observer. The static observer is located at event P with orthonormal tetrad $\{\hat{e}_{\hat{t}}, \hat{e}_{\hat{r}}, \hat{e}_{\hat{\theta}}, \hat{e}_{\hat{\phi}}\}$ as defined in Appendix B. For

the static observer, the black hole shadow occupies an angular radius θ_{crit} in the sky. This radius decreases with increasing coordinate distance r_O : at the black hole horizon itself, it encompasses the full sky; at the photon sphere, it subtends exactly half the sky ($\theta_{\text{crit}} = \pi/2$); and it diminishes asymptotically to zero [93].

We systematically investigate static, stable, spherically symmetric thin shells characterized by the parameter set $(m_{\pm}, \Lambda_{\pm}, \lambda, w_0)$, and construct a stability chart identifying the allowed parameter region and the corresponding equilibrium radius and surface energy density (R_0, σ_0) for each configuration. Throughout this analysis we fix $\lambda = 1$, which does not alter the magnitude of the deviations but determines the allowed stability range of w_0 . We consider the parameter ratios $m_+/m_- = 1.001$ and $\Lambda_+/\Lambda_- = 1.001$, and adopt a supermassive black hole mass $m_- = 10^{10} M_{\odot}$. The exterior cosmological constant Λ_+ is set according to Planck measurements, such that $\rho_{\Lambda_+} = \rho_{\text{crit}}$ [86]. With this configuration, we analyze its impact on the shadow angular radius for a static observer located at radial coordinate r_O , quantifying the deviation relative to the corresponding spacetime without a dark fluid shell (see Eq. (46)).

To study light geodesics, we introduce an affine parameter ζ and restrict our attention to the equatorial plane $\theta = \pi/2$. From the geodesic equation and the null condition $ds_{\pm}^2 = 0$, we derive the equations of motion:

$$\frac{dt_{\pm}}{d\zeta} = \frac{k_{\pm}}{f_{\pm}(r_{\pm})}, \quad (47)$$

$$\frac{d\phi}{d\zeta} = \frac{h_{\pm}}{r_{\pm}^2}, \quad (48)$$

$$c^2 k_{\pm}^2 - \frac{h_{\pm}^2}{r_{\pm}^2} f_{\pm}(r_{\pm}) = \left(\frac{dr_{\pm}}{d\zeta} \right)^2, \quad (49)$$

where k_{\pm} and h_{\pm} are constants of integration.

We determine the *angular radius* of the shadow for a static observer by introducing an orthonormal tetrad adapted to the observer's local rest frame [93]. Consider a static observer O at $\theta_O = \pi/2$. When the observer is inside the shell ($r_- = r_O < R_0$) and the shell itself lies outside the inner photon orbit $R_0 > 3Gm_-/c^2$ (as found for the static, stable configurations discussed in the previous section), we obtain (see Appendix B)[93, 94]

$$\sin^2 \theta_{\text{crit}}^- = \frac{f_-(r_O) (b_{\text{crit}}^-)^2}{r_O^2}. \quad (50)$$

The critical impact parameter b_{crit}^- corresponds to the threshold between trajectories that plunge into the black hole and those that scatter away. Note that for $r_- = 3Gm_-/c^2$, corresponding to the circular photon orbit (see Eq. (B21)), the critical impact parameter is given by

$$b_{\text{crit}}^- = \frac{3\sqrt{3}Gm_-}{c^2 \sqrt{1 - \frac{9G^2 m_-^2 \Lambda_-}{c^4}}}. \quad (51)$$

From the metric in Eq. (1), evaluated at the shell position $(t_{\pm}(\tau), r_{\pm} = R(\tau))$ and assuming a static shell ($\dot{R} = 0$), we have

$$\left(\frac{dt_+}{dt_-} \right)^2 = \frac{f_-(R)}{f_+(R)} \implies \frac{dt_+}{dt_-} = \sqrt{\frac{f_-(R)}{f_+(R)}}. \quad (52)$$

Moreover, when the radial coordinate is evaluated at the shell ($r_{\pm} = R$), Eq. (48) implies $h_+ = h_- = h$. Using Eqs. (47) and (52), we find the relation between the impact parameters:

$$\frac{b_+}{b_-} = \frac{k_-}{k_+} = \frac{f_-(R)}{f_+(R)} \frac{dt_-}{dt_+} = \sqrt{\frac{f_-(R)}{f_+(R)}}. \quad (53)$$

For an observer located exactly at the shell ($r_O = R$), and using Eq. (53), we obtain

$$\sin^2 \theta_{R,\text{crit}}^{\pm} = \frac{f_-(R) (b_{\text{crit}}^-)^2}{R^2} = \frac{f_+(R) (b_{\text{crit}}^+)^2}{R^2}. \quad (54)$$

Finally, for an observer outside the shell ($r_+ = r_O > R$), we have

$$\sin^2 \theta_{\text{crit}}^+ = \frac{f_+(r_O) (b_{\text{crit}}^+)^2}{r_O^2} =$$

$$= \frac{f_+(r_O) f_-(R) (b_{\text{crit}}^-)^2}{f_+(R) r_O^2} = \frac{f_+(r_O) R^2}{f_+(R) r_O^2} \sin^2 \theta_{R,\text{crit}}^{\pm}. \quad (55)$$

Combining these results, the angular radius of the shadow as perceived by an observer at an arbitrary radial position r_O in relation to a static stable thin shell with radius R_0 :

$$\sin^2 \Theta_{\text{crit}} = \begin{cases} \frac{f_-(r_O) (b_{\text{crit}}^-)^2}{r_O^2} & \text{if } r_O \leq R_0 \\ \frac{f_+(r_O) R_0^2}{f_+(R) r_O^2} \sin^2 \theta_{R_0,\text{crit}}^{\pm} & \text{if } r_O > R_0 \end{cases} \quad (56)$$

We demonstrate that, in principle, the equation-of-state parameter w_0 of the static, stable dark fluid shell can be constrained via observational measurements of the critical angular radius. Both positive ($w_0 > 0$) and negative ($w_0 < 0$) values of the EoS parameter produce potentially observable effects, primarily for observers situated outside the dark-fluid thin shell. For $w_0 < 0$, however—as illustrated in Fig. 6—the relative difference $(\Theta_{\text{crit}} - \theta_{\text{crit}})/\theta_{\text{crit}}$ is small ($\sim 10^{-12}$) for fixed parameters (m_{\pm}, Λ_{\pm}) , a consequence of the scale of R_0 where it is near the static radius and its corresponding σ_0 (for example, when $\Lambda_+/\Lambda_- < 1$, near-static-radius shells with positive pressure still yield the same order of deviation, albeit with distinct behavior). Conversely, for $w_0 > 0$ and an observer near the black hole, the relative difference can reach 10^{-3} even for $m_+/m_- = 1.001$.

Finally, we contrast these results with the reference case θ_{crit} corresponding to $\rho_{\Lambda} = \rho_{\text{crit}}$ [86]. In Fig. 6a — where we consider static, stable shells close to the

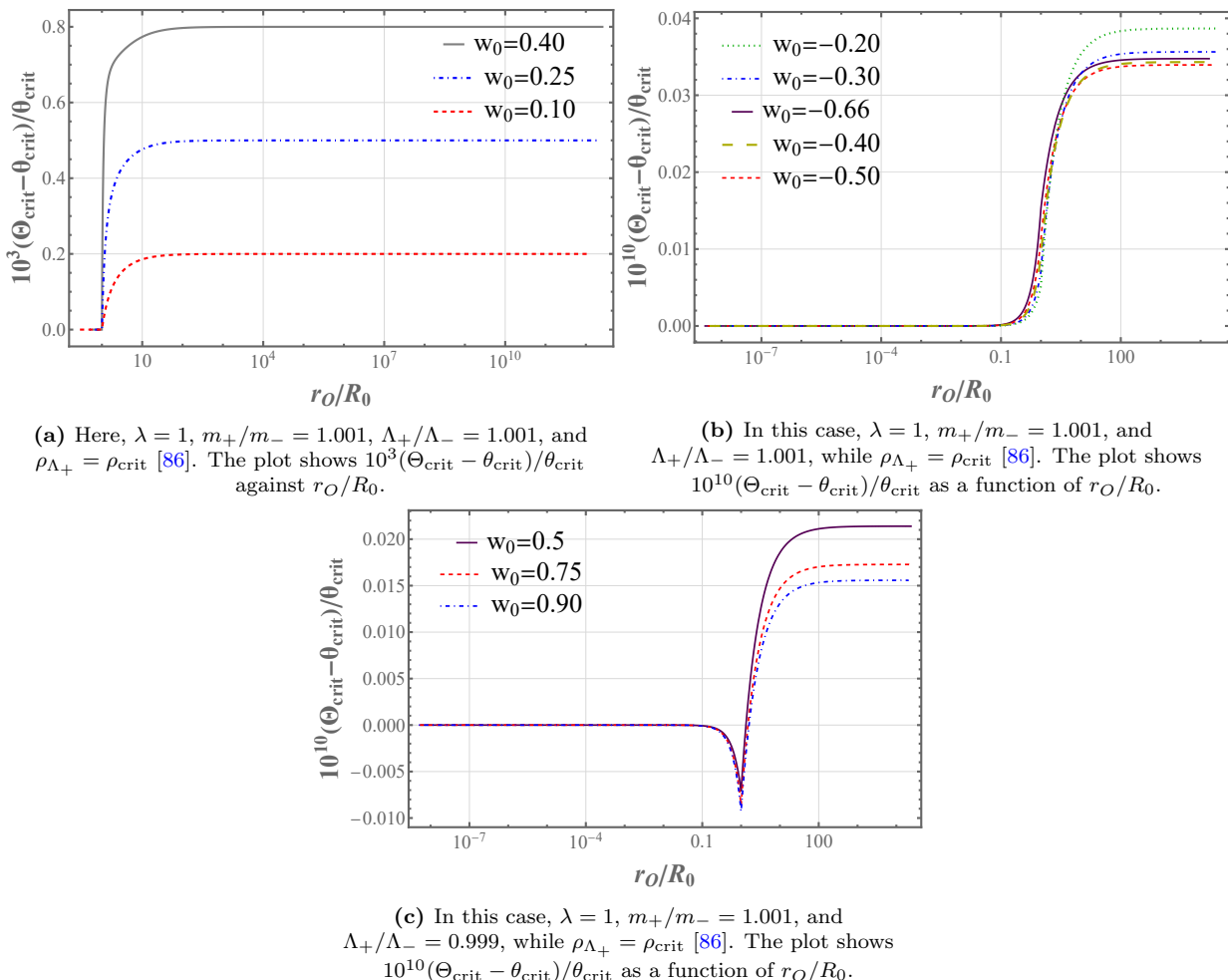


FIG. 6: Using Eqs. (46) and (56), we compute the critical angular radius of the shadow. For static, stable dark fluid shells near the photon sphere (case a), deviations are of order 10^{-3} , and larger values of w_0 allow the shells to approach even closer, producing significantly larger deviations in the shadow. In contrast, shells with negative or positive pressure for $w_0 > 0.5$, cases (b) and (c), which are near the static radius, produce smaller deviations. Note that, for negative-pressure shells, as w_0 decreases from 0 to $-1/2$, the deviation $\Theta_{\text{crit}} - \theta_{\text{crit}}$ initially decreases, reaching a minimum at $w_0 = -1/2$, and then increases again as w_0 approaches $-2/3$. For a static configuration at R_0 we have $\dot{R}_0 = \ddot{R}_0 = 0$. From Eq. (19), in the generic case ($w_0 \neq -\frac{1}{2}$) the shell's stress-energy explicitly enters the equilibrium condition. However, for $w_0 = -\frac{1}{2}$ the combination $\sigma_0 + 2p_0/c^2$ vanishes at R_0 , so the right-hand side of the dynamical junction equation is zero. The condition then reduces to continuity of the geometric term on the left-hand side, meaning that the shell does not contribute an additional active term to the force balance.

black hole so that gravitational attraction dominates over cosmological repulsion — the shadow changes very steeply. By contrast, in Fig. 6b (with $\Lambda = \Lambda_+ > \Lambda_-$, so that $\rho_{\Lambda_+} = \rho_{\Lambda} = \rho_{\text{crit}}$) the shell radii lie on the static (scale) radius: for radii smaller than the shell (and since $\Lambda_- < \Lambda$) the shadow increases smoothly and already begins to grow slightly before the static observer reaches the shell, because cosmological repulsion is not negligible. In Fig. 6c (where $\Lambda_- > \Lambda$) we again consider shells near the static radius; here the shadow initially deviates and becomes smaller for static observers located inside R_0 , and then increases beyond the shell — the overall amplitude of the effect is comparable to that in Fig. 6b but the detailed behaviour is distinct. Note that in the case of

Fig. 6b, for static observers located outside the shell and far from it, and considering negative-pressure shells, the deviation $\Theta_{\text{crit}} - \theta_{\text{crit}}$ initially decreases as w_0 decreases from 0 to $-\frac{1}{2}$, reaching a minimum at $w_0 = -\frac{1}{2}$, and then increases again as w_0 approaches $-\frac{2}{3}$. For a static configuration at R_0 , we have $\dot{R}_0 = \ddot{R}_0 = 0$ by definition. From Eq. (19), it is clear that for $w_0 = -\frac{1}{2}$ the combination $\sigma_0 + 2p_0/c^2$ vanishes. As a result, the right-hand side of the dynamical junction Eq. (19) becomes zero at R_0 . In this case, the condition reduces to the continuity of the geometric term on the left-hand side, implying that the shell does not contribute an additional active term to the force balance. In contrast, for the generic

case $w_0 \neq -\frac{1}{2}$ (and similarly for other values), the shell's stress-energy explicitly enters the equilibrium condition through its active gravitational mass.

Current EHT measurements of the M87* and Sgr A* shadow sizes carry fractional uncertainties at the few-percent level [113–116], so deviations of $\sim 10^{-3}$ lie roughly one order of magnitude below present sensitivity. However, next-generation space-based and ground-extended arrays are expected to reduce shadow size uncertainties to the sub-percent or even $\sim 10^{-3}$ level [114–119], placing positive-pressure shells near the photon sphere within the reach of future high-resolution campaigns. Shells near the static radius, by contrast, produce deviations twelve orders of magnitude smaller and are not constrained by any foreseeable shadow measurement.

V. CONCLUSION

In this work, we presented a detailed analysis of the existence and stability of static, spherically symmetric thin shells separating two Schwarzschild–de Sitter (SdS) spacetimes characterized by (m_{\pm}, Λ_{\pm}) . Using the Israel junction formalism and adopting a linearized equation of state $p = \lambda(\sigma - \sigma_1)c^2$, we decoupled the sound speed ($c_s^2 = \lambda c^2$) from the equilibrium equation-of-state parameter $w_0 \equiv p_0/(\sigma_0 c^2)$, enabling a more realistic description of the shell's microphysics even in the presence of negative pressure.

For a physically motivated example of a supermassive black hole ($\sim 10^{10} M_{\odot}$) and a cosmological constant of the order set by the Planck measurements [86], stable static configurations with positive surface energy density at R_0 and $0 < \lambda \leq 1$ exist only when $m_+/m_- > 1$. Equilibrium configurations are not confined to the near-horizon region of the black hole but can arise at three distinct characteristic scales: near the photon sphere, around the Schwarzschild–de Sitter static radius, and in the vicinity of the cosmological horizon.

A systematic stability analysis maps out the parameter space spanned by λ , w_0 , and the ratios m_+/m_- and Λ_+/Λ_- . Static, stable thin shells with $m_+ > m_-$ exist in the following cases, each with its corresponding maximum stability interval (attained for $\lambda = 1$):

- For $\Lambda_+ = \Lambda_-$, stability occurs in the range $-3/7 \lesssim w_0 \lesssim 1/2$. Positive-pressure shells reside near the photon sphere, while negative w_0 drives the shell smoothly toward the cosmological horizon.
- For $\Lambda_+ > \Lambda_-$, stability occurs for $-2/3 \lesssim w_0 \lesssim 1/2$. Positive-pressure shells remain near the photon sphere, while negative-pressure shells ($w_0 < 0$) extend outward only up to the static radius scale.
- For $\Lambda_+ < \Lambda_-$, stable shells exist for $0 \leq w_0 \leq 1$. Shells with $0 \lesssim w_0 \lesssim 1/2$ lie near the photon sphere with increasing R_0 . As $w_0 \rightarrow 1/2$, configurations

smoothly transition toward the static radius scale, while for $0.5 \lesssim w_0 \lesssim 1$, shells concentrate there as $w_0 \rightarrow 1$, with R_0 continuing to increase.

The equation-of-state parameter $w \equiv w(\sigma)$ can change sign as $\sigma(R)$ varies around R_0 , allowing stability through a combination of positive and negative pressures. For negative-pressure shells at R_0 , an outward radial perturbation reduces σ , increasing tension (more negative pressure) and pulling the shell inward, while inward perturbations weaken tension. Consequently, such shells must reside in a region of repulsive gravity to maintain equilibrium, or in a region of sufficiently weak attractive gravity such that an inward perturbation causes $w(\sigma)$ to increase rapidly enough (becoming positive) to counteract the gravitational pull on the shell. Positive-pressure shells behave analogously: contraction increases both σ and p , producing a restoring response, while expansion decreases them, requiring attractive gravity or sufficiently weak repulsive gravity where $w(\sigma)$ decreases rapidly enough to counteract the outward push.

Several astrophysical mechanisms can perturb a static thin shell away from equilibrium. Cosmological Hubble expansion, for instance, can quasi-statically shift equilibrium configurations away from their minima for shells located at scales $\sim R_{\text{st}}$ or larger. By perturbing the shell's effective potential, we consider small-energy perturbations (assumed not to backreact on the background spacetime) to gain insight into characteristic timescales. For example, when $m_+/m_- = 1.001$ and $\Lambda_+/\Lambda_- = 1.001$, with $m_- = 10^{10} M_{\odot}$ and $\rho_{\Lambda_+} = \rho_{\text{crit}}$ [86], a shell with $w_0 \simeq -2/3$ situated at $\sim 10^{21-22}$ m exhibits an oscillation period of order $\sim 10^{15}$ s when perturbed. If such a shell perturbed sufficiently, it will reach the cosmological horizon rather than collapse into the black hole.

The shell gravitationally magnifies the black hole shadow for a static observer located outside and far from it, with the magnitude of the deviation depending explicitly on the background parameters (m_{\pm}, Λ_{\pm}) , the equilibrium radius R_0 , and the equation-of-state parameter w_0 . The overall scale is primarily determined by (R_0, σ_0) (with σ_0 influencing it only indirectly through the junction conditions) and secondarily by the equation of state. Consequently, different physical configurations—such as negative- and positive-pressure shells located near the static radius—can produce shadow deviations of the same order, despite having opposite pressure signs. Thin shells are idealized toy models but may approximate realistic structures in two contexts, exotic phase transition boundaries where thickness is negligible, and dark matter spikes around supermassive black holes, where R_0 encodes the spike scale. While shells near the static radius yield undetectably small deviations ($\sim 10^{-12}$), positive-pressure shells near the photon sphere produce $\sim 10^{-3}$ deviations. As discussed in Sec. IV, this lies approximately one order of magnitude below the fractional precision of current EHT measurements, but falls within the projected sensitivity of next-generation space-based and extended ground arrays expected to achieve sub-percent to $\sim 10^{-3}$

shadow-size uncertainties [114–119]. Such observations could constrain steep dark matter spikes and, at least in principle, probe the imprints of phase transition boundaries at scales where their gravitational effect becomes observable.

ACKNOWLEDGMENTS

This research was supported by COST Action CA21136 - Addressing observational tensions in cosmology with systematics and fundamental physics (CosmoVerse), supported by COST (European Cooperation in Science and Technology). Furthermore, this work was supported by a scholarship from the University of Ioannina under the project “Enhancement and Support of the Operational, Research, and Educational Activities of the University of Ioannina” (Project Code: 82985/144059/ $\beta 6.\varepsilon$).

DATA AVAILABILITY STATEMENT

The figure-generating Mathematica (v13) and Python (3.12.12.) code will be publicly accessible in the GitHub repository and licensed under MIT in [123].

Appendix A: The Extrinsic Curvature as a 3-Tensor of the Hypersurface Σ

The projection tensor onto Σ is defined as (see [124])

$$P_{\mu\nu} = g_{\mu\nu} - \sigma n_\mu n_\nu, \quad (\text{A1})$$

where $\sigma \equiv n^\mu n_\mu$. The extrinsic curvature of Σ is defined via the Lie derivative of the projection tensor along the normal vector n^μ :

$$K_{\mu\nu} = \frac{1}{2} \mathcal{L}_n P_{\mu\nu} = \nabla_\mu n_\nu - \sigma n_\mu a_\nu, \quad (\text{A2})$$

where \mathcal{L}_n is the Lie derivative along n^μ and $a^\mu = n^\nu \nabla_\nu n^\mu$ is the acceleration of the integral curves of n^μ . Note that the spacetime extrinsic curvature restricted (projected) to the hypersurface Σ is

$$\hat{K}_{\alpha\beta} = P^\mu{}_\alpha P^\nu{}_\beta K_{\mu\nu} = P^\mu{}_\alpha P^\nu{}_\beta \nabla_\mu n_\nu. \quad (\text{A3})$$

Claim: The extrinsic curvature induced on Σ by pulling back \hat{K} from \mathcal{M} is

$$\mathcal{K}_{ij} \equiv [i^*(\hat{K})]_{ij} = [i^*(K)]_{ij} = \frac{\partial x^\mu}{\partial y^i} \frac{\partial x^\nu}{\partial y^j} \nabla_\mu n_\nu. \quad (\text{A4})$$

Proof: We define the extrinsic curvature on Σ as the pullback of the projected on Σ spacetime extrinsic curvature \hat{K} through the inclusion map $i : \Sigma \hookrightarrow \mathcal{M}$:

$$\mathcal{K}_{ij} \equiv [i^*(\hat{K})]_{ij}. \quad (\text{A5})$$

Note that at any point $p \in \Sigma$, the pushforward i_* maps a tangent vector $e_i \in T_p \Sigma$ to a tangent vector $i_* e_i \in T_{i(p)} \mathcal{M} = T_p \mathcal{M}$ in the spacetime \mathcal{M} . Let y^i be coordinates on the hypersurface Σ . The pushforward of the coordinate basis vectors $e_i = \partial/\partial y^i$ under the inclusion map $i : \Sigma \hookrightarrow \mathcal{M}$ is

$$i_*(e_i) = \frac{\partial x^\mu}{\partial y^i} \frac{\partial}{\partial x^\mu} \equiv e_i^\mu \frac{\partial}{\partial x^\mu}. \quad (\text{A6})$$

If ∂_μ denotes the coordinate basis on \mathcal{M} , then the projected on Σ spacetime extrinsic curvature evaluated on this basis is $\hat{K}(\partial_\mu, \partial_\nu) \equiv \hat{K}_{\mu\nu}$. By the definition of the pullback, for tangent vectors $e_i, e_j \in T_p \Sigma$ we have

$$[i^*(\hat{K})](e_i, e_j) = \hat{K}(i_* e_i, i_* e_j) = \hat{K}_{\mu\nu} e_i^\mu e_j^\nu. \quad (\text{A7})$$

Using $\hat{K}_{\mu\nu} = P^\alpha{}_\mu P^\beta{}_\nu \nabla_\alpha n_\beta$ and the fact that the pushforward components e_i^μ are tangent to Σ , so $P^\alpha{}_\mu e_i^\mu = e_i^\alpha$, one obtains [12]

$$\mathcal{K}_{ij} = \nabla_\alpha n_\beta e_i^\alpha e_j^\beta = \frac{\partial x^\alpha}{\partial y^i} \frac{\partial x^\beta}{\partial y^j} \nabla_\alpha n_\beta. \quad \square \quad (\text{A8})$$

Appendix B: The Schwarzschild-de Sitter Geometry

We consider a static, spherically symmetric black hole of mass m embedded in a universe with positive cosmological constant Λ . The unique solution to the vacuum Einstein equations $R_{\mu\nu} - \Lambda g_{\mu\nu} = 0$ with these symmetries is the Schwarzschild-de Sitter metric [125, 126]:

$$ds^2 = f(r) c^2 dt^2 - \frac{dr^2}{f(r)} - r^2 (d\theta^2 + \sin^2 \theta d\phi^2), \quad (\text{B1})$$

where $f(r)$ is given by:

$$f(r) = 1 - \frac{2Gm}{c^2 r} - \frac{\Lambda r^2}{3}. \quad (\text{B2})$$

We impose the condition $f(r) = 0$ and demand that this equation have three real solutions: two positive roots and one negative root. When this requirement is satisfied, the spacetime exhibits two physical horizons. The smaller of the positive roots corresponds to the black-hole horizon, which lies close to (for $\rho_\Lambda = \rho_{\text{crit}}$ [86])—but slightly outside—the Schwarzschild radius, while the larger positive root defines the cosmological horizon [127, 128].

1. Christoffel symbols

The nonvanishing Christoffel symbols associated with metric in Eq. (B1) are

$$\Gamma^t_{tr} = \frac{f'(r)}{2f(r)}, \quad \Gamma^r_{tt} = \frac{1}{2}f'(r)f(r), \quad (\text{B3})$$

$$\Gamma^r_{rr} = -\frac{f'(r)}{2f(r)}, \quad \Gamma^r_{\theta\theta} = -rf(r), \quad (\text{B4})$$

$$\Gamma^r_{\phi\phi} = -rf(r)\sin^2\theta, \quad \Gamma^\theta_{\phi\phi} = -\sin\theta\cos\theta, \quad (\text{B5})$$

$$\Gamma^\phi_{r\phi} = \Gamma^\theta_{r\theta} = \frac{1}{r}, \quad \Gamma^\phi_{\theta\phi} = \cot\theta. \quad (\text{B6})$$

2. The static radius R_{st}

A key feature of the SdS geometry is the existence of a unique radius at which the ‘‘gravitational forces’’ from the black hole and the cosmological constant exactly balance [129, 130]. To identify this radius, we examine the geodesic equation for a radially moving test particle.

We parameterize the timelike geodesic using an affine parameter τ . For motion confined to the equatorial plane $\theta = \pi/2$, the equations of motion are derived from the geodesic equation and the condition $ds^2 = c^2 d\tau^2$ as [131]:

$$\dot{t} = \frac{k}{f(r)}, \quad (\text{B7})$$

$$\dot{\phi} = \frac{h}{r^2}, \quad (\text{B8})$$

$$c^2(k^2 - 1) = \dot{r}^2 + \frac{h^2}{r^2}f(r) + c^2[f(r) - 1], \quad (\text{B9})$$

By taking the derivative of Eq. (B9) with respect to the proper time τ , we find:

$$0 = \frac{d^2r}{d\tau^2} - \frac{h^2}{r^3}f(r) + \frac{h^2}{2r^2}\frac{df}{dr} + \frac{c^2}{2}\frac{df}{dr}. \quad (\text{B10})$$

For purely radial motion of a massive particle, the angular momentum must vanish, i.e. $h = 0$. Equation (B10) then reduces to

$$\frac{d^2r}{d\tau^2} = -c^2 \left(\frac{Gm}{c^2 r^2} - \frac{\Lambda r}{3} \right). \quad (\text{B11})$$

The radial acceleration vanishes when

$$r = R_{\text{st}} \equiv \left(\frac{3Gm}{\Lambda c^2} \right)^{1/3}. \quad (\text{B12})$$

At this distance, a test particle initially at rest experiences no net force and therefore remains at rest indefinitely.

3. Lightlike trajectories in Schwarzschild-de Sitter spacetime

We parameterize the null geodesic using an affine parameter λ . For motion confined to the equatorial plane $\theta = \pi/2$, the equations of motion are derived from the geodesic equation and the null condition $ds^2 = 0$ as [131]:

$$\dot{t} = \frac{k}{f(r)}, \quad (\text{B13})$$

$$\dot{\phi} = \frac{h}{r^2}, \quad (\text{B14})$$

$$c^2 k^2 = \dot{r}^2 + \frac{h^2}{r^2}f(r), \quad (\text{B15})$$

where $\dot{\cdot} \equiv d/d\lambda$ and k, h integration constants. By setting as

$$b \equiv h/(ck),$$

the energy Eq. (B15) can be rewritten as

$$\frac{\dot{r}^2}{2} + V_{\text{eff}}(r) = \frac{h^2}{2b^2}, \quad (\text{B16})$$

where

$$V_{\text{eff}}(r) = \frac{h^2}{2r^2} \left(1 - \frac{2Gm}{c^2 r} - \frac{\Lambda}{3} r^2 \right). \quad (\text{B17})$$

The shape equation of the photon orbit is obtained via Eq. (B15) as

$$\left(\frac{dr}{d\phi} \right)^2 = \frac{1}{b^2} r^4 - r^2 f(r). \quad (\text{B18})$$

Introducing the impact parameter $b \equiv h/(ck)$, the spatial trajectory $r(\phi)$ depends only on b and on the metric function $f(r)$. Consequently, fixing b uniquely determines the spatial trajectory $r(\phi)$ up to trivial degeneracies: (i) a constant shift $\phi \mapsto \phi + \phi_0$, corresponding to a rotation about the symmetry axis, (ii) a choice of sign for $dr/d\phi$, selecting ingoing or outgoing branches of the same orbit, and (iii) an affine reparametrization of the worldline, since simultaneous rescalings (k, h) leave b invariant and merely rescale the affine parameter (see Eqs. (B13)-(B14)). Thus, a fixed value of b labels an equivalence class (family) of null geodesics that share the same spatial path and differ only by initial conditions or parameterization.

Now, by introducing the substitution $u \equiv 1/r$ into Eq. (B18) and then differentiating with respect to the azimuthal angle ϕ , we obtain the second-order differential equation

$$\frac{d^2u}{d\phi^2} = \frac{3Gm}{c^2} u^2 - u. \quad (\text{B19})$$

Setting $u = u_0$ and $du/d\phi = d^2u/d\phi^2 = 0$ we obtain the radius of the circular photon orbit as

$$r_0 = \frac{3Gm}{c^2}. \quad (\text{B20})$$

The circular light ray at $r = 3Gm/c^2$ is unstable. A small perturbation of the photon's initial trajectory in the equatorial plane will cause it to depart from this circular path and ultimately cross either the inner or outer horizon. Moreover, we rewrite Eq. (B18) as

$$\frac{dr}{d\phi} = \pm r^2 \left(\frac{1}{b^2} - \frac{1}{r^2} + \frac{2Gm}{c^2 r^3} + \frac{\Lambda}{3} \right)^{1/2}. \quad (\text{B21})$$

The critical value $b = b_{\text{crit}}$ corresponds to the threshold between trajectories that plunge into the black hole and those that scatter away. Note that if we set as $r = r_0$ then Eq. (B21) yields

$$b_{\text{crit}} = \frac{3\sqrt{3}Gm}{c^2 \sqrt{1 - \frac{9G^2 m^2 \Lambda}{c^4}}}. \quad (\text{B22})$$

4. Shadow of the SdS black hole for a static observer

We determine the angular radius of the shadow for a static observer in Schwarzschild–de Sitter (SdS) space-time by introducing an orthonormal tetrad adapted to the observer's local rest frame [93]. For a static observer O , at $\theta_O = \pi/2$, the four-velocity has only a t -component,

$$[u_O^\mu] = (u_O^t, 0, 0, 0). \quad (\text{B23})$$

Imposing the normalization condition $g_{\mu\nu}u^\mu u^\nu = c^2$ yields

$$g_{tt}(u_O^t)^2 = c^2 \quad \Rightarrow \quad f(r)(u_O^t)^2 = c^2, \quad (\text{B24})$$

from which we obtain

$$u_O^t = \frac{c}{\sqrt{f(r_O)}}. \quad (\text{B25})$$

The observer's orthonormal tetrad vectors [124, 131] are chosen as

$$(\hat{e}_t)^\mu = \frac{u_O^\mu}{c}, \quad (\hat{e}_r)^\mu = \left(0, \sqrt{f(r_O)}, 0, 0 \right), \quad (\text{B26})$$

together with the angular basis vectors

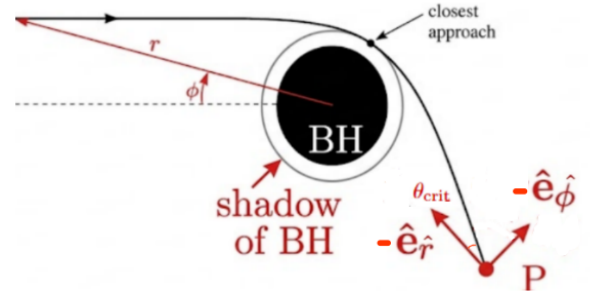
$$(\hat{e}_\theta)^\mu = \left(0, 0, \frac{1}{r_O}, 0 \right), \quad (\hat{e}_\phi)^\mu = \left(0, 0, 0, \frac{1}{r_O \sin \theta_O} \right). \quad (\text{B27})$$

Note that the metric satisfies

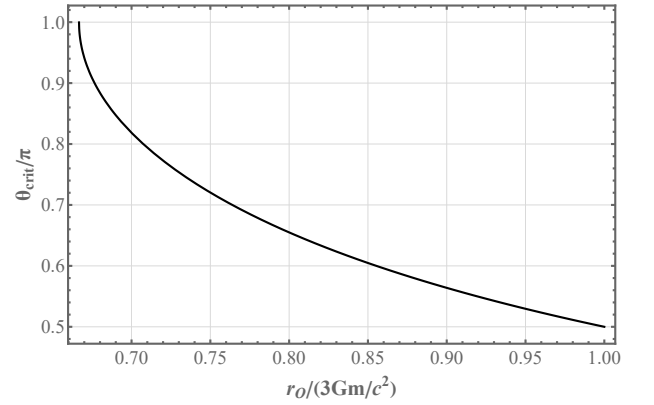
$$g_{\mu\nu}(\hat{e}_a)^\mu (\hat{e}_b)^\nu = \eta_{\hat{a}\hat{b}}$$

with $[\eta_{\hat{a}\hat{b}}] = \text{diag}(1, -1, -1, -1)$. When the observer's worldline intersects that of a photon confined to the equatorial plane $\vartheta = \pi/2$ with coordinate four-momentum

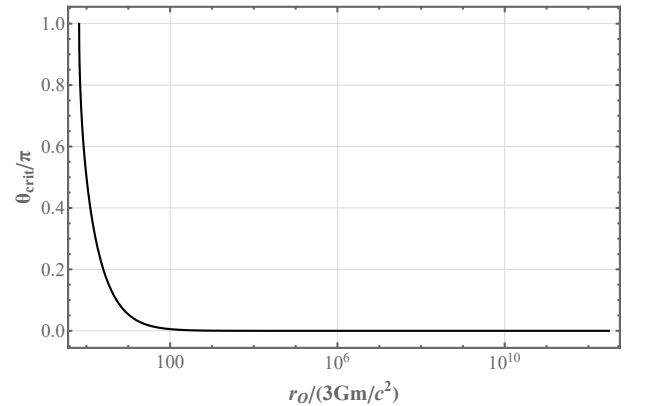
$$[p^\mu] = \left(\frac{k}{f}, \dot{r}, 0, \frac{h}{r^2} \right),$$



(a) The figure schematically depicts the projected black hole shadow in the equatorial (r, ϕ) plane. The parity-inverted orientation (a left-handed frame) is used only for visual convenience. The observer is located at event P with orthonormal tetrad $\{\hat{e}_t, \hat{e}_r, \hat{e}_\theta, \hat{e}_\phi\}$ as defined in the text. For clarity of illustration, the spatial axes shown in the figure are the **negatives** of the tetrad's spatial basis vectors: $-\hat{e}_r$ (pointing radially inward toward the black hole) and $-\hat{e}_\phi$ (pointing westward).



(b) We plot the normalized critical angle θ_{crit}/π as a function of the observer's radial coordinate r_O , considering the range from the inner black hole horizon out to the photon orbit ($\theta_{\text{crit}} = \pi/2$) (see also [94]). The cosmological constant density is set to $\rho_\Lambda = \rho_{\text{crit}}$ [86], and the black hole mass is taken as $m = 10^{10} M_\odot$.



(c) We plot the normalized critical angle θ_{crit}/π as a function of the observer's radial coordinate r_O (logarithmic scale), considering the range from the inner black hole horizon out to the cosmological horizon. The cosmological constant density is set to $\rho_\Lambda = \rho_{\text{crit}}$ [86], and the black hole mass is taken as $m = 10^{10} M_\odot$.

FIG. 7: The Black Hole Shadow as Perceived by a Static Observer

at an event P , projecting the photon four-momentum onto the static observer's orthonormal tetrad at $r = r_O$ gives the following. The projections of p^μ are then

$$p_{\hat{t}} = g_{\mu\nu} p^\mu (\hat{e}_{\hat{t}})^\nu = \frac{k}{\sqrt{f(r_O)}}, \quad (\text{B28})$$

$$p_{\hat{r}} = g_{\mu\nu} p^\mu (\hat{e}_{\hat{r}})^\nu = -\frac{\dot{r}|_O}{\sqrt{f(r_O)}}, \quad (\text{B29})$$

$$p_{\hat{\phi}} = g_{\mu\nu} p^\mu (\hat{e}_{\hat{\phi}})^\nu = -\frac{h}{r_O}. \quad (\text{B30})$$

Note that the observer measures the photon direction from the spatial 3-vector $\mathbf{p} = (p^{\hat{r}}, 0, p^{\hat{\phi}})$. The angular radius θ_* of the shadow (angle between the photon's spatial direction and the radial inward direction) may be taken from the ratio of the orthonormal spatial components (see Fig. 7a):

$$\tan \theta_* = \frac{|p^{\hat{\phi}}|}{|p^{\hat{r}}|}.$$

Using the projected components above we get

$$\tan \theta_* = \frac{h\sqrt{f(r_O)}}{r_O |\dot{r}|_{r=r_O}}. \quad (\text{B31})$$

Writing $dr/d\varphi = \dot{r}/\dot{\varphi} = \dot{r}/(h/r^2)$ we have

$$|\dot{r}| = \frac{h}{r^2} \left| \frac{dr}{d\varphi} \right|,$$

and substituting into (B31) yields

$$\tan^2 \theta_* = \frac{r_O^2 f(r_O)}{\left(\frac{dr}{d\varphi} \right)_{r=r_O}^2}.$$

We substitute the Eq. (B21) and we get

$$\tan^2 \theta_* = \frac{f(r_O)}{\frac{1}{b^2} r_O^2 - f(r_O)}.$$

Using $\sin^2 \theta = \frac{\tan^2 \theta}{1 + \tan^2 \theta}$ one finds after simplifying

$$\sin^2 \theta_* = \frac{f(r_O) b^2}{r_O^2}.$$

Substituting the corresponding critical impact parameter (Eq. (B22)), we obtain the angular radius of the shadow as measured by a static observer at r_O [92–94]:

$$\sin^2 \theta_{\text{crit}} = \frac{1 - \frac{2Gm}{c^2 r_O} - \frac{\Lambda r_O^2}{3}}{r_O^2 \left(\frac{c^4}{27G^2 m^2} - \frac{\Lambda}{3} \right)}. \quad (\text{B32})$$

For the static observer, the black hole shadow occupies an angular radius θ_{crit} in the sky. This radius decreases with increasing coordinate distance r_O (see Fig. 7): at the horizon itself, it encompasses the full sky; at the photon sphere, it subtends exactly half the sky ($\theta_{\text{crit}} = \pi/2$); and it diminishes asymptotically to zero [93].

-
- [1] P. LeMaitre and E. Poisson, *Am. J. Phys.* **87**, 961 (2019), [arXiv:1909.06253 \[gr-qc\]](#).
- [2] A. Vilenkin, *Phys. Rev. D* **23**, 852 (1981).
- [3] L. Perivolaropoulos, *Phys. Rev. D* **97**, 124035 (2018), [arXiv:1804.08098 \[gr-qc\]](#).
- [4] G. Alestas, G. V. Kraniotis, and L. Perivolaropoulos, *Phys. Rev. D* **102**, 104015 (2020), [arXiv:2005.11702 \[gr-qc\]](#).
- [5] I. Antoniou, D. Kazanas, D. Papadopoulos, and L. Perivolaropoulos, *Int. J. Mod. Phys. D* **31**, 2250064 (2022), [arXiv:2204.14003 \[gr-qc\]](#).
- [6] G. Alestas and L. Perivolaropoulos, *Phys. Rev. D* **99**, 064026 (2019), [arXiv:1901.06659 \[gr-qc\]](#).
- [7] L. Randall and R. Sundrum, *Phys. Rev. Lett.* **83**, 3370 (1999).
- [8] I. Antoniadis, N. Arkani-Hamed, S. Dimopoulos, and G. R. Dvali, *Phys. Lett. B* **436**, 257 (1998), [arXiv:hep-ph/9804398](#).
- [9] N. Arkani-Hamed, S. Dimopoulos, and G. R. Dvali, *Phys. Lett. B* **429**, 263 (1998), [arXiv:hep-ph/9803315](#).
- [10] W. Israel, *Nuovo Cim. B* **44S10**, 1 (1966), [Erratum: *Nuovo Cim. B* 48, 463 (1967)].
- [11] J. Kijowski, G. Magli, and D. Malafarina, *General Relativity and Gravitation* **38**, 1697 (2006).
- [12] E. Poisson, *A Relativist's Toolkit: The Mathematics of Black-Hole Mechanics* (Cambridge University Press, 2009).
- [13] O. y. Grøn and S. Hervik, *Einstein's General Theory of Relativity: With Modern Applications in Cosmology*, 1st ed. (Springer, New York, 2007).
- [14] J. Frauendiener, C. Hoenselaers, and W. Konrad, *Class. Quant. Grav.* **7**, 585 (1990).
- [15] P. R. Brady, J. Louko, and E. Poisson, *Phys. Rev. D* **44**, 1891 (1991).
- [16] B. G. Schmidt, *Phys. Rev. D* **59**, 024005 (1999).
- [17] K. G. Zloshchastiev, *Int. J. Mod. Phys. D* **8**, 549 (1999), [arXiv:gr-qc/9802041](#).
- [18] R. Chan, M. F. A. da Silva, and P. Rocha, *JCAP* **12**, 017, [arXiv:0910.2054 \[gr-qc\]](#).
- [19] J. P. Pereira, J. G. Coelho, and J. A. Rueda, *Phys. Rev. D* **90**, 123011 (2014), [arXiv:1412.1848 \[gr-qc\]](#).
- [20] S. Pradhan, D. Mohanty, and P. K. Sahoo, *Chin. Phys.*

- C **47**, 095104 (2023), arXiv:2306.17435 [gr-qc].
- [21] M. Visser and D. L. Wiltshire, *Class. Quant. Grav.* **21**, 1135 (2004), arXiv:gr-qc/0310107.
- [22] P. Pani, E. Berti, V. Cardoso, Y. Chen, and R. Norte, *Phys. Rev. D* **80**, 124047 (2009), arXiv:0909.0287 [gr-qc].
- [23] V. Berezin, V. Kuzmin, and I. Tkachev, *Physics Letters B* **120**, 91 (1983).
- [24] P. Laguna-Castillo and R. A. Matzner, *Phys. Rev. D* **34**, 2913 (1986).
- [25] V. A. Berezin, V. A. Kuzmin, and I. I. Tkachev, *Phys. Rev. D* **36**, 2919 (1987).
- [26] M. Ishak and K. Lake, *Phys. Rev. D* **65**, 044011 (2002), arXiv:gr-qc/0108058.
- [27] S. M. C. V. Goncalves, *Phys. Rev. D* **66**, 084021 (2002), arXiv:gr-qc/0212124.
- [28] F. S. N. Lobo and P. Crawford, *Class. Quant. Grav.* **22**, 4869 (2005), arXiv:gr-qc/0507063.
- [29] S. Habib Mazharimousavi, M. Halilsoy, and S. N. Hamad Amen, *Int. J. Mod. Phys. D* **26**, 1750158 (2017), arXiv:1708.04588 [gr-qc].
- [30] A. D. D. Masa, E. S. de Oliveira, and V. T. Zanchin, *Phys. Rev. D* **103**, 104051 (2021), arXiv:2009.10948 [gr-qc].
- [31] M. Cataldo, A. Cid, and P. Labraña, *Eur. Phys. J. C* **85**, 1461 (2025), arXiv:2512.13575 [gr-qc].
- [32] J. Crisostomo, S. del Campo, and J. Saavedra, *Phys. Rev. D* **70**, 064034 (2004), arXiv:hep-th/0311259.
- [33] J. Crisostomo and R. Olea, *Phys. Rev. D* **69**, 104023 (2004), arXiv:hep-th/0311054.
- [34] P. Bueno, P. A. Cano, R. A. Hennigar, and Á. J. Murcia, *Phys. Rev. D* **111**, 104009 (2025), arXiv:2412.02740 [gr-qc].
- [35] A. G. Schubert, *Entropy* **28**, 10.3390/e28010096 (2026).
- [36] E. Gravanis and S. Willison, *Phys. Rev. D* **75**, 084025 (2007), arXiv:gr-qc/0701152.
- [37] F. Javed, J. Lin, G. Mustafa, and F. M. O. Tawfiq, *Fortsch. Phys.* **72**, 2300081 (2024).
- [38] H. Beauchesne and A. Edery, *Phys. Rev. D* **85**, 044056 (2012), arXiv:1108.0449 [gr-qc].
- [39] F. Javed, *Eur. Phys. J. C* **83**, 513 (2023).
- [40] A. Hussain, F. Javed, G. Fatima, F. Tchier, S. Nozima, and G. Mustafa, *Int. J. Geom. Meth. Mod. Phys.* **22**, 2450297 (2025).
- [41] P. Musgrave and K. Lake, *Class. Quant. Grav.* **13**, 1885 (1996), arXiv:gr-qc/9510052.
- [42] R. J. Gleiser and M. A. Ramirez, *Class. Quant. Grav.* **26**, 045006 (2009), arXiv:0807.4728 [gr-qc].
- [43] E. F. Eiroa and C. Simeone, *Phys. Rev. D* **83**, 104009 (2011), arXiv:1102.1683 [gr-qc].
- [44] L. M. Reyes, M. Chiapparini, and S. E. P. Bergliaffa, *Eur. Phys. J. C* **82**, 151 (2022).
- [45] S. Habib Mazharimousavi and M. Halilsoy, *Eur. Phys. J. C* **73**, 2527 (2013), arXiv:1305.2909 [gr-qc].
- [46] S. H. Mazharimousavi and M. Halilsoy, *Eur. Phys. J. C* **75**, 334 (2015), arXiv:1503.05587 [gr-qc].
- [47] J. P. S. Lemos and G. M. Quinta, *Phys. Rev. D* **88**, 067501 (2013), arXiv:1309.1478 [gr-qc].
- [48] J. P. S. Lemos and G. M. Quinta, *Phys. Rev. D* **89**, 084051 (2014), arXiv:1403.0579 [gr-qc].
- [49] E. F. Eiroa, E. Rubín de Celis, and C. Simeone, *Eur. Phys. J. C* **76**, 546 (2016), arXiv:1608.04729 [gr-qc].
- [50] E. Poisson and M. Visser, *Phys. Rev. D* **52**, 7318 (1995), arXiv:gr-qc/9506083.
- [51] F. S. N. Lobo and P. Crawford, *Class. Quant. Grav.* **21**, 391 (2004), arXiv:gr-qc/0311002.
- [52] F. S. N. Lobo, in *APCTP Winter School and Workshop on Quantum Gravity, Black Holes and Wormholes* (2004) arXiv:gr-qc/0401083.
- [53] F. S. N. Lobo, *Class. Quant. Grav.* **21**, 4811 (2004), arXiv:gr-qc/0409018.
- [54] E. F. Eiroa and C. Simeone, *Phys. Rev. D* **76**, 024021 (2007), arXiv:0704.1136 [gr-qc].
- [55] J. P. S. Lemos and F. S. N. Lobo, *Phys. Rev. D* **78**, 044030 (2008), arXiv:0806.4459 [gr-qc].
- [56] G. A. S. Dias and J. P. S. Lemos, *Phys. Rev. D* **82**, 084023 (2010), arXiv:1008.3376 [gr-qc].
- [57] N. M. Garcia, F. S. N. Lobo, and M. Visser, *Phys. Rev. D* **86**, 044026 (2012), arXiv:1112.2057 [gr-qc].
- [58] K.-i. Nakao, T. Uno, and S. Kinoshita, *Phys. Rev. D* **88**, 044036 (2013), arXiv:1306.6917 [gr-qc].
- [59] M. Sharif and M. Azam, *JCAP* **04**, 023, arXiv:1305.4441 [gr-qc].
- [60] N. Tsukamoto and T. Kokubu, *Phys. Rev. D* **98**, 044026 (2018), arXiv:1807.01528 [gr-qc].
- [61] A.-C. Li, W.-L. Xu, and D.-F. Zeng, *JCAP* **03**, 016, arXiv:1812.07224 [hep-th].
- [62] Z. Amirabi, *Eur. Phys. J. C* **79**, 410 (2019).
- [63] T. Berry, F. S. N. Lobo, A. Simpson, and M. Visser, *Phys. Rev. D* **102**, 064054 (2020), arXiv:2008.07046 [gr-qc].
- [64] F. S. N. Lobo, G. J. Olmo, E. Orazi, D. Rubiera-Garcia, and A. Rustam, *Phys. Rev. D* **102**, 104012 (2020), arXiv:2009.10997 [gr-qc].
- [65] F. S. N. Lobo, A. Simpson, and M. Visser, *Phys. Rev. D* **101**, 124035 (2020), arXiv:2003.09419 [gr-qc].
- [66] M. Sharif and F. Javed, *Phys. Scripta* **96**, 055003 (2021).
- [67] J. L. Rosa, R. André, and J. P. S. Lemos, *Gen. Rel. Grav.* **55**, 65 (2023), arXiv:2305.06829 [gr-qc].
- [68] A. Eid, A. Alkaoud, M. M. Khader, and M. A. Bakry, *Sci. Rep.* **14**, 12696 (2024).
- [69] A. Eid, *New Astron.* **98**, 101934 (2023).
- [70] F. S. N. Lobo, *Universe* **11**, 270 (2025), arXiv:2508.17823 [gr-qc].
- [71] T. S. Rippenrop, A. Bera, and M. Ishak, *Phys. Rev. D* **112**, 124069 (2025), arXiv:2507.00315 [gr-qc].
- [72] G. Antoniou, A. Papageorgiou, and P. Kanti, *Universe* **9**, 147 (2023), arXiv:2210.17533 [gr-qc].
- [73] N. Sakai, H. Saida, and T. Tamaki, *Phys. Rev. D* **90**, 104013 (2014), arXiv:1408.6929 [gr-qc].
- [74] J. Peng, M. Guo, and X.-H. Feng, *Phys. Rev. D* **104**, 124010 (2021), arXiv:2102.05488 [gr-qc].
- [75] K.-J. He, Z. Luo, S. Guo, and G.-P. Li, *Chin. Phys. C* **48**, 065105 (2024).
- [76] L.-M. Cao, L.-Y. Li, and X.-Y. Liu, arXiv:2511.13077 [gr-qc] (2025).
- [77] R. Saleem, N. Aslam, and M. Israr Aslam, *Nucl. Phys. B* **1022**, 117251 (2026).
- [78] C. F. B. Macedo, J. L. Rosa, D. Rubiera-Garcia, and A. Rueda, *Multi-photon ring structure of reflection-asymmetric traversable thin-shell wormholes* (2025), arXiv:2510.19677 [gr-qc].
- [79] A. Laeuger, C. Weller, D. Li, and Y. Chen, *Phys. Rev. D* **112**, 084042 (2025), arXiv:2506.00367 [gr-qc].
- [80] B. Wu, E.-W. Liang, and X. Zhang, *Eur. Phys. J. C* **85**, 632 (2025), arXiv:2501.00361 [gr-qc].
- [81] J. Ben Achour, E. Gourgoulhon, and H. Roussille, *JCAP*

- 10**, 012, arXiv:2506.09882 [gr-qc].
- [82] L. Perivolaropoulos, I. Antoniou, and D. Papadopoulos, *Mon. Not. Roy. Astron. Soc.* **524**, 1246 (2023), arXiv:2302.12524 [gr-qc].
- [83] S.-W. Kim, *Physics Letters A* **166**, 13 (1992).
- [84] E. Babichev, V. Dokuchaev, and Y. Eroshenko, *Class. Quant. Grav.* **22**, 143 (2005), arXiv:astro-ph/0407190.
- [85] E. Babichev, V. Dokuchaev, and Y. Eroshenko, *Phys. Rev. Lett.* **93**, 021102 (2004), arXiv:gr-qc/0402089.
- [86] N. Aghanim *et al.* (Planck), *Astronomy & Astrophysics* **641**, A6 (2020), arXiv:1807.06209.
- [87] L. Perivolaropoulos and F. Skara, *New Astron. Rev.* **95**, 101659 (2022), arXiv:2105.05208 [astro-ph.CO].
- [88] E. F. Eiroa and G. Figueroa Aguirre, *Eur. Phys. J. C* **76**, 132 (2016), arXiv:1511.02806 [gr-qc].
- [89] V. Faraoni and A. Jacques, *Phys. Rev. D* **76**, 063510 (2007), arXiv:0707.1350 [gr-qc].
- [90] A. Einstein and E. G. Straus, *Rev. Mod. Phys.* **17**, 120 (1945).
- [91] R. Balbinot, R. Bergamini, and A. Comastri, *Phys. Rev. D* **38**, 2415 (1988).
- [92] V. Perlick and O. Y. Tsupko, *Phys. Rept.* **947**, 1 (2022), arXiv:2105.07101 [gr-qc].
- [93] Z. Stuchlík and S. Hledík, *Phys. Rev. D* **60**, 044006 (1999).
- [94] V. Perlick, O. Y. Tsupko, and G. S. Bisnovatyi-Kogan, *Phys. Rev. D* **97**, 104062 (2018), arXiv:1804.04898 [gr-qc].
- [95] G. Bertone, *Nucl. Phys. B* **1003**, 116487 (2024), arXiv:2404.11513 [astro-ph.CO].
- [96] P. J. E. Peebles, *General Relativity and Gravitation* **3**, 63 (1972), revised 25 August 1971.
- [97] P. Young, *The Astrophysical Journal* **242**, 1232 (1980).
- [98] W. Dehnen, *Mon. Not. Roy. Astron. Soc.* **265**, 250 (1993).
- [99] G. D. Quinlan, L. Hernquist, and S. Sigurdsson, *Astrophys. J.* **440**, 554 (1995), arXiv:astro-ph/9407005.
- [100] P. Gondolo and J. Silk, *Phys. Rev. Lett.* **83**, 1719 (1999), arXiv:astro-ph/9906391.
- [101] L. Sadeghian, F. Ferrer, and C. M. Will, *Phys. Rev. D* **88**, 063522 (2013), arXiv:1305.2619 [astro-ph.GA].
- [102] D. Efstratiou and L. Perivolaropoulos, *Phys. Rev. D* **111**, 123546 (2025), arXiv:2503.11365 [gr-qc].
- [103] L. Perivolaropoulos and F. Skara, *Phys. Rev. D* **106**, 043528 (2022), arXiv:2203.10374 [astro-ph.CO].
- [104] Y. B. Zeldovich, I. Y. Kobzarev, and L. B. Okun, *Zh. Eksp. Teor. Fiz.* **67**, 3 (1974).
- [105] T. W. B. Kibble, *J. Phys. A* **9**, 1387 (1976).
- [106] S. R. Coleman, *Phys. Rev. D* **15**, 2929 (1977), [Erratum: *Phys.Rev.D* 16, 1248 (1977)].
- [107] C. G. Callan, Jr. and S. R. Coleman, *Phys. Rev. D* **16**, 1762 (1977).
- [108] S. R. Coleman and F. De Luccia, *Phys. Rev. D* **21**, 3305 (1980).
- [109] A. Vilenkin, *Phys. Rept.* **121**, 263 (1985).
- [110] X. Dong and D. Harlow, *JCAP* **11**, 044, arXiv:1109.0011 [hep-th].
- [111] E. Babichev, D. Gorbunov, S. Ramazanov, and A. Vikman, *JCAP* **04** (04), 028, arXiv:2112.12608 [hep-ph].
- [112] D. Wei and Y. Jiang, *Phys. Rev. D* **110**, 123505 (2024), arXiv:2208.07186 [hep-ph].
- [113] P. Galison *et al.*, *Galaxies* **11**, 32 (2023), arXiv:2304.02463 [physics.hist-ph].
- [114] A. W. Raymond *et al.* (Event Horizon Telescope), *Astron. J.* **168**, 130 (2024), arXiv:2410.07453 [astro-ph.IM].
- [115] V. Kudriashov, M. Martin-Neira, F. Roelofs, H. Falcke, C. Brinkerink, A. Baryshev, M. Hogerheijde, A. Young, H. Pourshaghghi, M. Klein-Wolt, M. Moscibrodzka, J. Davelaar, I. Barat, B. Duesmann, V. Valenta, A. J. M. Perdignes, D. de Wilde, I. P. Martin, N. Alagha, and D. V. M. van, *Chinese Journal of Space Science* **41**, 211 (2021), arXiv:2105.06882 [astro-ph.IM].
- [116] K. Akiyama *et al.* (Event Horizon Telescope), *Astron. Astrophys.* **704**, A91 (2025), arXiv:2509.24593 [astro-ph.HE].
- [117] X. Hong, W. Wu, Q. Liu, D. Yu, C. Wang, T. Shuai, W. Zhong, R. Zhu, Y. Xie, L. Zhang, L. Xiong, Y. Tang, Y. Zou, H. Li, G. Wang, J. Xie, C. Xue, H. Geng, J. Zhang, X. Wu, Y. Huang, W. Zheng, L. Liu, F. Wu, X. Zhang, T. An, X. Yang, F. Tong, L. I. Gurvits, Y. Zheng, M. Gu, X. Ma, L. Li, P. Li, S. Zhao, P. Rui, L. Chen, G. Chen, K. Li, C. Zhang, Y. Liu, Y. Jiang, J. Wang, W. Wang, Y. Sun, L. Hao, L. Cui, D. Jiang, Z. Qian, and S. Ye, *Science China Physics, Mechanics, and Astronomy* **69**, 219511 (2025), arXiv:2507.16317 [astro-ph.IM].
- [118] T. Mroczkowski *et al.*, *Astron. Astrophys.* **694**, A142 (2025), arXiv:2402.18645 [astro-ph.IM].
- [119] K. Akiyama *et al.*, arXiv:2602.04666 [astro-ph.IM] (2026).
- [120] E. A. Paraskevas and L. Perivolaropoulos, *Phys. Rev. D* **112**, 043524 (2025), arXiv:2505.08603 [quant-ph].
- [121] E. A. Paraskevas and L. Perivolaropoulos, *Universe* **11**, 62 (2025), arXiv:2502.07929 [gr-qc].
- [122] V. I. Arnold, *Mathematical Methods of Classical Mechanics*, Graduate Texts in Mathematics (Springer, 1989).
- [123] D. Efstratiou, *Static thin shells in sds-spacetimes* (2026).
- [124] S. M. Carroll, *Spacetime and Geometry: An Introduction to General Relativity* (Cambridge University Press, 2019).
- [125] F. Kottler, *Annalen der Physik* **361**, 401 (1918).
- [126] H. Weyl, *Physikalische Zeitschrift* **20**, 31 (1919).
- [127] G. W. Gibbons and S. W. Hawking, *Physical Review D* **15**, 2738 (1977).
- [128] R. Bousso, *Reviews of Modern Physics* **74**, 825 (2002), arXiv:hep-th/0203101.
- [129] Z. Stuchlík and S. Hledík, *Classical and Quantum Gravity* **17**, 4541 (2000).
- [130] A. Balaguera-Antolínez, C. G. Böhrer, and M. Nowakowski, *Classical and Quantum Gravity* **23**, 485 (2006), arXiv:gr-qc/0511057.
- [131] M. P. Hobson, G. P. Efstathiou, and A. N. Lasenby, *General Relativity: An Introduction for Physicists* (Cambridge University Press, Cambridge, 2006).